MtNODULE ROOT1 and MtNODULE ROOT2 Are Essential for Indeterminate Nodule Identity

Kevin Magne, Jean-Malo Couzigou, Katharina Schiessl, Shengbin Liu, Jeoffrey George, Vladimir Zhukov, Lucien Sahl, Frédéric Boyer, Anelia Iantcheva, Kirankumar S Mysore, et al.

MtNODULE ROOT1 and *MtNODULE ROOT2* Are Essential for Indeterminate Nodule Identity[1][OPEN]

Kevin Magne,[a,b] Jean-Malo Couzigou,[a,b,2] Katharina Schiessl,[c] Shengbin Liu,[a,b] Jeoffrey George,[a,b,3] Vladimir Zhukov,[d] Lucien Sahl,[a,b] Frederic Boyer,[a,b] Anelia Iantcheva,[e] Kirankumar S. Mysore,[f] Jiangqi Wen,[f] Sylvie Citerne,[g] Giles E.D. Oldroyd,[c] and Pascal Ratet[a,b,4,5]

[a]Institute of Plant Sciences Paris-Saclay IPS2, Centre National de la Recherche Scientifique, Institut National de la Recherche Agronomique, Université Paris-Sud, Université Evry, Université Paris-Saclay, Bâtiment 630, 91405 Orsay, France
[b]Institute of Plant Sciences Paris-Saclay IPS2, Paris Diderot, Sorbonne Paris-Cité, Bâtiment 630, 91405 Orsay, France
[c]Department of Cell and Developmental Biology, John Innes Centre, Norwich NR4 7UH, United Kingdom
[d]ARRIAM, Laboratory of Genetics of Plant-Microbe Interactions, Podbelsky chaussée 3, 196608 Pushkin, St. Petersburg, Russia
[e]AgroBioInstitute, 1164 Sofia, Blvd.Dragan Tzankov 8, Bulgaria
[f]Plant Biology Division, Samuel Roberts Noble Foundation, Ardmore, Oklahoma 73401
[g]Institut Jean-Pierre Bourgin, Institut National de la Recherche Agronomique, AgroParisTech, Centre National de la Recherche Scientifique, Université Paris-Saclay, 78000 Versailles, France

ORCID IDs: 0000-0002-6779-5683 (K.M.); 0000-0002-7694-0619 (K.S.); 0000-0001-7512-4225 (S.L.); 0000-0002-6018-8602 (J.G.); 0000-0002-2411-9191 (V.Z.); 0000-0001-8491-7040 (A.I.); 0000-0002-9805-5741 (K.S.M.); 0000-0001-5113-7750 (J.W.); 0000-0001-5026-095X (S.C.); 0000-0002-5245-6355 (G.E.O.); 0000-0002-8621-1495 (P.R.)

Symbiotic interactions between legume plants and rhizobia result in the formation of nitrogen-fixing nodules, but the molecular actors and the mechanisms allowing for the maintenance of nodule identity are poorly understood. *Medicago truncatula NODULE ROOT1* (*MtNOOT1*), *Pisum sativum COCHLEATA1* (*PsCOCH1*), and *Lotus japonicus NOOT-BOP-COCH-LIKE1* (*LjNBCL1*) are orthologs of Arabidopsis (*Arabidopsis thaliana*) *AtBLADE-ON-PETIOLE1/2* and are members of the *NBCL* gene family, which has conserved roles in plant development and is essential for indeterminate and determinate nodule identity in legumes. The loss of function of *MtNOOT1*, *PsCOCH1*, and *LjNBCL1* triggers a partial loss of nodule identity characterized by the development of ectopic roots arising from nodule vascular meristems. Here, we report the identification and characterization of a second gene involved in regulating indeterminate nodule identity in *M. truncatula*, *MtNOOT2*. *MtNOOT2* is the paralog of *MtNOOT1* and belongs to a second legume-specific *NBCL* subclade, the *NBCL2* clade. *MtNOOT2* expression was induced during early nodule formation, and it was expressed primarily in the nodule central meristem. *Mtnoot2* mutants did not present any particular symbiotic phenotype; however, the loss of function of both *MtNOOT1* and *MtNOOT2* resulted in the complete loss of nodule identity and was accompanied by drastic changes in the expression of symbiotic, defense, and root apical meristem marker genes. *Mtnoot1 noot2* double mutants developed only nonfixing root-like structures that were no longer able to host symbiotic rhizobia. This study provides original insights into the molecular basis underlying nodule identity in legumes forming indeterminate nodules.

The symbiotic interaction between legumes and rhizobia results in the formation of root nodules dedicated to host nitrogen-fixing rhizobia. This unique ability to form root nodules is restricted to the Rosids I clade. The predisposition of plants to enter symbiosis with nitrogen-fixing rhizobia seems to have evolved once, between 70 and 100 million years ago, and to have derived from an ancestral and widespread symbiosis, the arbuscular mycorrhizal symbiosis (Soltis et al., 1995; Smith and Read, 2008; Bonfante and Genre, 2010; Humphreys et al., 2010; Werner et al., 2014).

Genetic approaches using nodule-deficient (nod$^-$) and nonfunctional nodule (fix$^-$) mutant plants allowed the identification of many genes essential for the early steps of root nodule symbiosis. Recognition between symbiotic partners, rhizobial infection, and nodule organogenesis are initiated by the host plant perception of rhizobial lipochitooligosacharidic compounds (Lerouge et al., 1990; Jones et al., 2007; Oldroyd and Downie, 2008; Kouchi et al., 2010; Horvath et al., 1993; Ovchinnikova et al., 2011; Oldroyd, 2013; Udvardi and Poole, 2013; Suzaki et al., 2015). These compounds are called Nod factors, and they are structurally similar to the mycorrhization factors required for arbuscular mycorrhizal symbiosis initiation (Maillet et al., 2011).

In the Papilionaceae family, determinate nodules formed in the Phaseoleae, Loteae, and Dalbergieae tribes have no persistent apical nodule meristem (NM). However, indeterminate nodules formed in the Trifolieae and Fabeae tribes have a persistent apical NM. Indeterminate nodules are highly structured and present different zones: the NM, the infection zone, the nitrogen

fixation zone, and the older senescent zone (from top to bottom; Vasse et al., 1990). The ability of indeterminate nodules to grow continuously results from the presence of the NM.

In the model legume *Medicago truncatula* (Trifolieae) forming indeterminate nodules, root developmental regulators such as *MtWUSCHEL-RELATED-HOMEOBOX5* (*MtWOX5*) and the *APETALA2/ethylene response factors* (*AP2/ERF*) *MtPLETHORA1* (*MtPLT1*) to *MtPLT4* transcription factors (TFs) are expressed in the NM. The presence of such regulators in the NM suggests that a root-derived program is active in this meristematic zone (Osipova et al., 2011, 2012; Roux et al., 2014; Franssen et al., 2015). In the literature, the analysis of *PromoterMtWOX5*, *PromoterMtPLT1* to *PromoterMtPLT4*, synthetic auxin response element DR5 and synthetic cytokinin-dependent promoter, and the two-component signaling sensor GUS reporter fusions revealed the composite nature of the NM. The *M. truncatula* NM is composed of distinct meristematic subdomains: a single nodule central meristem (NCM) surrounded by multiple nodule vascular meristems (NVMs; Osipova et al., 2011, 2012; Couzigou et al., 2013; Roux et al., 2014; Franssen et al., 2015). These meristematic subdomains have distinct origins; NVMs derive from the root pericycle and endodermis cell layers, while the NCM derives from the third root cortex cell layer (Couzigou et al., 2012; Xiao et al., 2014).

Despite these important advances in our understanding of NM organization, the molecular mechanisms and the molecular actors involved in NM regulation remain poorly described and misunderstood.

NOOT-BOP-COCH-LIKE (*NBCL*) genes encode transcriptional cofactors that are orthologous to Arabidopsis (*Arabidopsis thaliana*) *AtBLADE-ON-PETIOLE1/2* (*AtBOP1/2*; Ha et al., 2003, 2004; Hepworth et al., 2005; Norberg et al., 2005). NBCL proteins contain BROAD COMPLEX, TRAMTRACK, and BRICK A BRACK/POXVIRUSES and ZINC FINGER (BTB/POZ) and ANKYRIN repeat domains. These proteins are essential plant developmental regulators and act mainly through the regulation of the plant boundaries and the promotion of lateral organ differentiation (for review, see Khan et al., 2014; Žádníková and Simon, 2014; Hepworth and Pautot, 2015; Wang et al., 2016). In addition to their roles in plant development, legume NBCL genes are required for nodule identity regulation and the control of NVM activity. Indeed, in both indeterminate and determinate nodule-forming species, the loss of function of *M. truncatula MtNODULEROOT1* (*MtNOOT1*), *Pisum sativum PsCOCHLEATA1* (*PsCOCH1*), and *Lotus japonicus LjNOOT-BOP-COCH-LIKE1* (*LjNBCL1*) genes triggers the development of ectopic roots initiating from NVMs (Ferguson and Reid, 2005; Couzigou et al., 2012, 2013; Couzigou and Ratet, 2015; Magne et al., 2018).

In this work, we report the identification and characterization of a gene involved in *M. truncatula* nodule identity regulation, the *MtNODULE ROOT2* (*MtNOOT2*) gene. *MtNOOT2* is the paralog of *MtNOOT1* and belongs to a legume-specific *NBCL* subclade that we called *NBCL2*. The *MtNOOT2* gene expression profile is characteristic because *MtNOOT2* expression was induced during nodule formation and associated with the NCM from early nodule primordium stages.

We provide evidence that *MtNOOT2* is essential for *M. truncatula* indeterminate nodule identity regulation along with *MtNOOT1*. While *MtNOOT2* loss of function did not alter either nodule development or identity, the *Mtnoot1 noot2* double mutant showed a complete loss of nodule identity characterized by a complete nodule-to-root identity reversion. *Mtnoot1 noot2* was no longer able to develop structured indeterminate nodules and was unable to host symbiotic rhizobia. The nodule-to-root homeosis was accompanied

[1]This work was supported by the CNRS, by Agence National de la Recherche Grants ANR SVSE 6.2010.1 (LEGUMICS) and ANR-14-CE19-0003 (NOOT) to P.R., by The Russian Science Foundation Grant 17-76-30016 to V.Z., and by the Bill and Melinda Gates Foundation to G.E.D.O. J.-M.C. was supported by a PhD fellowship from the French Ministry of Research and the French Academy of Agriculture (Dufrenoy Grant, 2011). This work benefited from the facilities and expertise of the IMAGIF Cell Biology Unit of the Gif campus (www.imagif.cnrs.fr), which is supported by the Conseil Général de l'Essonne. The Institute of Plant Sciences Paris-Saclay (IPS2) benefits from the support of the LabEx Saclay Plant Sciences-SPS (ANR-10-LABX-0040-SPS).

[2]Current address: Laboratoire de Recherche en Sciences Végétales, Université de Toulouse, Centre National de la Recherche Scientifique, UPS, 24 chemin de Borde Rouge, Auzeville, BP42617, 31326 Castanet Tolosan, France.

[3]Current address: Sainsbury Laboratory, Norwich Research Park, Norwich NR4 7UH, UK.

[4]Author for contact: pascal.ratet@u-psud.fr.

[5]Senior author.

The author responsible for distribution of materials integral to the findings presented in this article in accordance with the policy described in the instructions for authors (www.plantphysiol.org) is: Pascal Ratet (pascal.ratet@u-psud.fr).

P.R., K.M., J.M.C., K.S., and G.E.D.O. conceived the project; K.M. performed the phylogenetic analysis, RT-qPCR analyses, in situ RNA hybridization, histological analysis, eGFP bacteria localization, and yeast two-hybrid experiments and generated *Mtnoot1/ProNOOT2:GUS* and *Mtnoot2/ProNOOT1:GUS* transgenic lines by crossing; J.-M.C. generated *Mtnoot1 noot2* double mutants by crossing; J.-M.C. and V.Z. constructed *ProNOOT1:GUS* and *ProNOOT2:GUS* fusions; A.I. produced *ProNOOT2:GUS* stable transformants in *M. truncatula* R-108; K.M., J.-M.C., V.Z., and J.G. performed in toto *ProNOOT1:GUS* and *ProNOOT2:GUS* analyses; K.M., S.L., and J.G. performed *ProNOOT1:GUS* and *ProNOOT2:GUS* fusion histological analyses; K.M., J.-M.C., J.G., L.S., and F.B. performed *Mtnoot* simple and double mutant nodule phenotyping and performed acetylene reduction assays; K.M. and S.C. performed salicylic acid quantifications; K.S. constructed the *ProKNOX9:GUS* fusion, performed *ProKNOX9:GUS* hairy root transformations, and analyzed *ProKNOX9:GUS* expression patterns; K.S.M., J.W., and P.R. generated the *M. truncatula Tnt1* mutant collection and performed the *Mtnoot* mutant screens; K.M., J.-M.C., K.S., S.L., J.G., L.S., F.B., A.I., K.S.M., J.W., V.Z., S.C., G.E.D.O., and P.R. analyzed the data; K.M., K.S., and P.R. wrote the article.

[OPEN]Articles can be viewed without a subscription.

www.plantphysiol.org/cgi/doi/10.1104/pp.18.00610

by a drastic gene expression reprogramming, especially a down-regulation of symbiotic marker genes and an up-regulation of both defense and root developmental marker genes. The complete loss of nodule identity in *Mtnoot1 noot2* finally resulted in a nonfunctional symbiosis and in the absence of nitrogen fixation.

RESULTS

NBCL2, a Legume-Specific *NBCL* Subclade

A BLAST analysis (https://blast.ncbi.nlm.nih.gov/) using the *MtNOOT1* sequence as a query revealed the existence of an NBCL paralog in *M. truncatula* genomes (R-108 and Jemalong). This *NBCL* gene was cloned and named *MtNOOT2* according to the literature (Couzigou et al., 2012). *MtNOOT2* was found later to correspond to Medtr1g051025 in the *M. truncatula* genome version Mt4.0 (Benedito et al., 2008; He et al., 2009; Tang et al., 2014). In *P. sativum*, the ortholog of *MtNOOT2* also was found, cloned, and named *PsCOCH2* according to the literature (Wellensiek, 1959; Blixt, 1967; Gourlay et al., 2000; Yaxley et al., 2001; Couzigou et al., 2012). In addition to *M. truncatula* and *P. sativum*, *MtNOOT1* and MtNOOT2 orthologs were found in other legume species such as common bean (*Phaseolus vulgaris*; *Pv*NBCL1 and *Pv*NBCL2), chickpea (*Cicer arietinum*; *Ca*NBCL1 and *Ca*NBCL2), pigeon pea (*Cajanus cajan*; *Cc*NBCL1 and *Cc*NBCL2), soybean (*Glycine max*; *Gm*NBCLa, *Gm*NBCLb, and *Gm*NBCLc; (Couzigou et al., 2016), *L. japonicus* (*Lj*NBCL1; Couzigou et al., 2016; Magne et al., 2018), and narrow-leafed lupine (*Lupinus angustifolius*; *La*NBCL1, *La*NBCL2a, and *La*NBCL2b; Frankowski et al., 2015; Couzigou et al., 2016).

To better understand legume NBCL protein evolution, we compared legume NBCL protein sequences with NBCL protein sequences from nonlegume plants of different families (Brassicaceae, Solanaceae, Poaceae, and Zosteraceae). Our phylogenetic analysis revealed that the legume NBCL proteins divided into two legume-specific NBCL subclades, hereafter called NBCL1 and NBCL2 subclades (Fig. 1; Supplemental Table S1). We found that all legume *Mt*NOOT1 and *Mt*NOOT2 orthologs grouped in the NBCL1 and NBCL2 subclades, respectively. In NBCL1 and NBCL2 subclades, NBCL sequences were highly conserved and showed a minimum of 74% and 78% identity, respectively (Fig. 1). A detailed alignment of six legume NBCL2 sequences revealed the high conservation of both the BTB/POZ and ANKYRIN repeat domains (Supplemental Fig. S1).

Except for *L. japonicus*, which seems to have lost its NBCL2 ortholog (Magne et al., 2018), it appears that legume species, in general, have retained at least two distinct NBCL paralogs (Fig. 1).

MtNOOT2 Expression Behaves Similarly to the Symbiotic Gene *MtNODULE INCEPTION*

To better understand the role of the *MtNOOT* genes during symbiosis, we quantified the accumulation of *MtNOOT1* and *MtNOOT2* transcripts in *M. truncatula* R-108 roots, root apical meristems (RAMs), and nodules by reverse transcription quantitative PCR (RT-qPCR).

According to previous studies, *MtNOOT1* transcripts accumulate in roots and nodules but fewer transcripts are detected in the RAM (Fig. 2A; Couzigou et al., 2012). In *Sinorhizobium medicae* WSM419 (WSM419) inoculated roots, *MtNOOT1* expression decreased slightly from 2 to 5 d post inoculation (dpi). A similar *MtNOOT1* expression decrease also was reported in Nod factor-treated roots (Herrbach et al., 2017). During nodule development, from 8 to 21 dpi, *MtNOOT1* expression increased (Fig. 2A).

In contrast to *MtNOOT1*, *MtNOOT2* transcripts were not detectable in roots, the RAM, and inoculated roots from 0 to 5 dpi. *MtNOOT2* transcripts started to accumulate once nodule primordia had developed at 8 dpi and continued to accumulate during nodule development until 21 dpi (Fig. 2A). In *P. sativum*, which also produces indeterminate nodules, the *PsCOCH2* expression profile was similar to that of *MtNOOT2* (PsGene Expression Atlas [http://bios.dijon.inra.fr/FATAL/cgi/pscam.cgi]; Alves-Carvalho et al., 2015). Thus, once the nodule primordium starts to develop, *MtNOOT1* and *MtNOOT2* transcripts accumulate, with *MtNOOT1* transcripts accumulating to higher levels compared with *MtNOOT2* (Fig. 2A).

To better understand the kinetics of MtNOOT2 expression during nodulation, its expression was compared with the expression of marker genes known to be sequentially repressed or induced during the symbiotic process. In agreement with previous studies, after inoculation, *MtPATHOGENESIS RELATED-PROTEIN10* (*MtPR10*) was induced early in roots at 2 dpi, and its expression decreased at 5 dpi and became undetectable after 8 dpi (Fig. 2B; Bourcy et al., 2013b). *MtLEGHEMOGLOBIN1* (*MtLEGH1*) transcripts were detectable from 5 dpi and accumulated strongly after 8 dpi. Transcripts of the early symbiotic gene *MtNODULE INCEPTION* (*MtNIN*) were detected between 5 and 8 dpi and were induced strongly in nodules. We found that MtNOOT2 gene expression behaved in a similar manner to that of *MtNIN* (Fig. 2B). *MtNODULE SPECIFIC CYSTEINE RICH PEPTIDE001* (*MtNCR001*) transcripts were detected later, from 8 to 21 dpi (Fig. 2B).

These results indicate that *MtNOOT2* behaves as a symbiotic gene, and the different *MtNOOT1* and *MtNOOT2* expression profiles indicate that they may have distinct roles during nodule organogenesis.

MtNOOT1 Is Expressed in Developing Nodule Vascular Bundles

To precisely define the spatial and temporal expression pattern of *MtNOOT1* during nodule development, stable transgenic plants expressing *PromoterMtNOOT1:GUS*

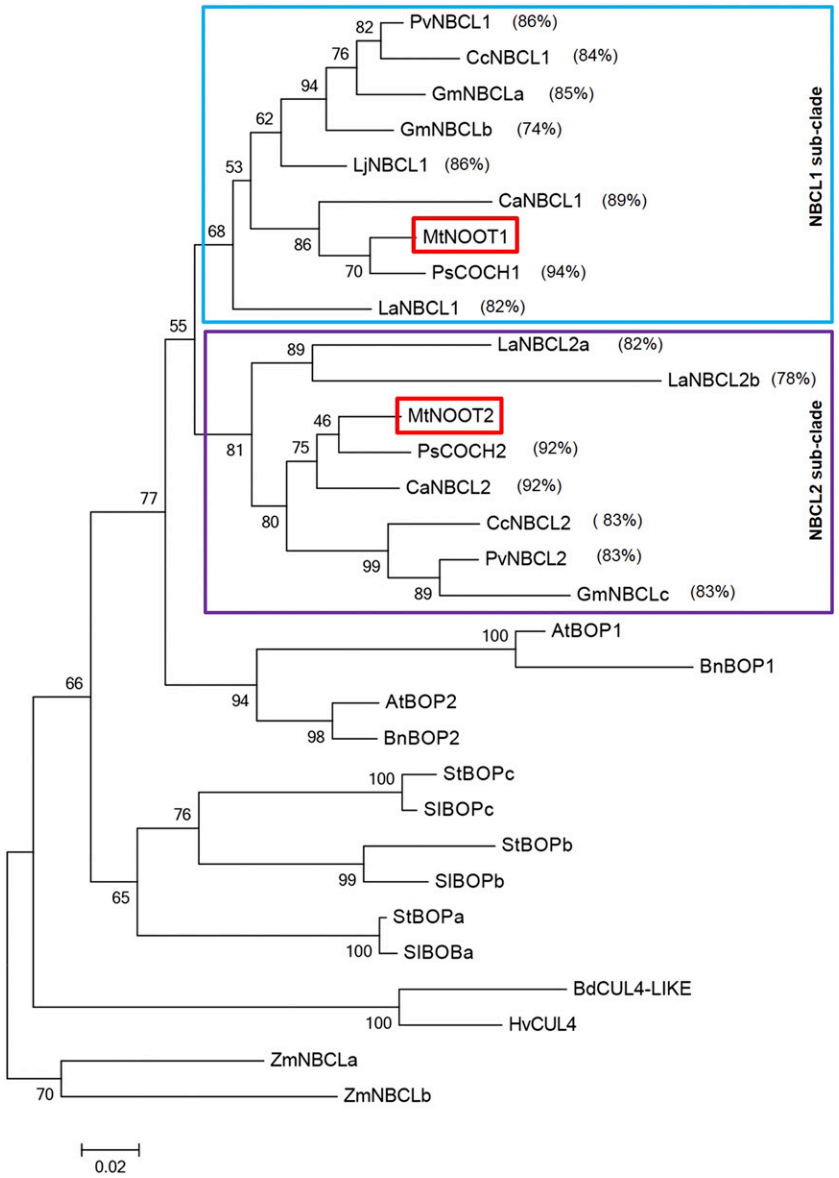

Figure 1. Maximum likelihood-based phylogenetic tree of NBCL proteins. NBCL sequences are from Fabaceae, *M. truncatula* (Mt; red frames), *Pisum sativum* (Ps), *Phaseolus vulgaris* (Pv), *Cicer arietinum* (Ca), *Lupinus angustifolius* (La), *Cajanus cajan* (Cc), *Glycine max* (Gm), and *Lotus japonicus* (Lj); from Brassicaceae, *Arabidopsis thaliana* (At) and *Brassica napus* (Bn); from Solanaceae, *Solanum lycopersicum* (Sl) and *Solanum tuberosum* (St); and from Poaceae, *Hordeum vulgare* (Hv) and *Brachypodium distachyon* (Bd). The tree is rooted with NBCL sequences from the basal monocot *Zostera marina* (Zm). Light blue and dark purple frames indicate the legume NBCL1- and NBCL2-specific subclades, respectively. Percentage values indicate the identity percentage of the legume NBCL1 and NBCL2 proteins relative to MtNOOT1 and MtNOOT2, respectively. Evolutionary divergence scale bars represent 0.02 substitution per site. Detailed information concerning NBCL protein sequences used in this phylogenetic analysis is provided in Supplemental Table S1.

(*ProNOOT1*:*GUS*; Couzigou et al., 2012) were used. In these transgenic plants, *ProNOOT1*:*GUS* is constitutively expressed in the root stele (Couzigou et al., 2012).

Nodule primordium stages were defined according to Xiao et al. (2014). In nodule primordium stages III and IV, characterized by anticlinal divisions in the third cortex cell layer (C3) and the endodermis and periclinal divisions in the endodermis and pericycle (Fig. 3A), and in nodule primordium stage V, characterized by the presence of anticlinal divisions in the second cortex cell layer (C2) and the presence of multiple cell layers derived from C3 (Fig. 3B), the *ProNOOT1*:*GUS* fusion was not expressed and remained undetectable

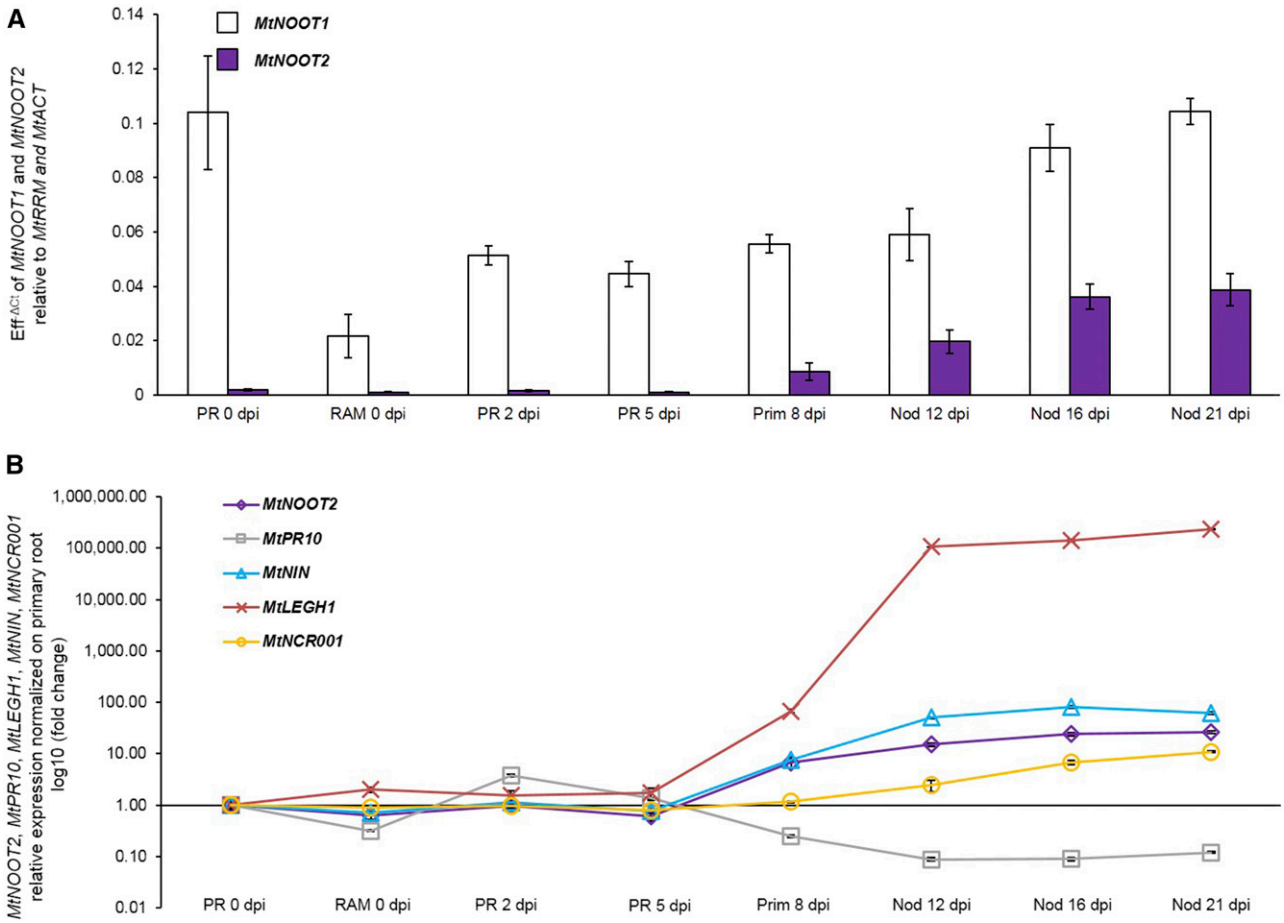

Figure 2. *MtNOOT1* and *MtNOOT2* expression and comparison with marker gene expression during nodulation. A, RT-qPCR gene expression analysis of *MtNOOT1* (white bars) and *MtNOOT2* (purple bars) transcript accumulation. B, RT-qPCR gene expression analysis of *MtNOOT2* (purple diamonds) compared with the gene expression of the nodulation marker genes *MtPR10* (gray squares), *MtLEGH1* (red crosses), *MtNIN* (blue triangles), and *MtNCR001* (orange circles). RT-qPCR gene expression analysis was performed in uninoculated primary roots devoid of RAM (2 d post stratification: primary root [PR] 0 dpi), in uninoculated RAM (0.5 cm, 2 d post stratification: RAM 0 dpi), in inoculated primary root (PR 2, 5 dpi), in nodule primordia (Prim 8 dpi) and in nodules (Nod 12, 16, and 21 dpi) inoculated with WSM419. In A, *MtNOOT1* and *MtNOOT2* expression levels were normalized against the constitutively expressed genes *MtRNA RECOGNITION MOTIF* (*MtRRM*) and *MtACTIN* (*MtACT*). In B, *MtNOOT2*, *MtPR10*, *MtLEGH1*, *MtNIN*, and *MtNCR001* expression levels were normalized against the constitutively expressed *MtRRM* and *MtACT* genes and against uninoculated primary root at 0 dpi. The *y* axis represents $\log_{10}$ fold change. All results represent means ± SE of four biological replicates and three technical replicates.

in root stele, where the future nodule will develop (Fig. 3, A and B).

In early nodule stage VI, characterized by the presence of approximatively six basal cell layers derived from pericycle and endodermis cells, *ProNOOT1*:*GUS* expression was detected in pericycle- and endodermis-derived cell layers (Fig. 3C). In young nodules, *ProNOOT1*:*GUS* was expressed strongly but restricted to nodule vascular bundles (NVBs), including nodule vascular pericycle and endodermis tissues derived from root pericycle and endodermis cell layers (Fig. 3D). At later stages of nodule development, *ProNOOT1*:*GUS* expression was highly dynamic but was essentially associated with the developing NVB and reduced in older parts of the NVB (Fig. 3, E and F; Supplemental Fig. S2A).

Detailed histological analyses focusing on the NVM/NCM boundary region showed that *ProNOOT1*:*GUS* was associated mostly with the nodule vascular pericycle and endodermis cells, as described previously (Fig. 3, G and H; Couzigou et al., 2012). In addition, *ProNOOT1*:*GUS* transcripts were never detected in the NCM, in the nodule infection zone, in the nodule fixation zone, in the nodule parenchyma, in the nodule endodermis, and in the nodule cortex (Fig. 3, C–H).

Based on the organization of indeterminate NVBs (;Pate,1976;Guinel,2009),weshowedthat*ProNOOT1*:*GUS* expression was restricted to NVB cells, including the

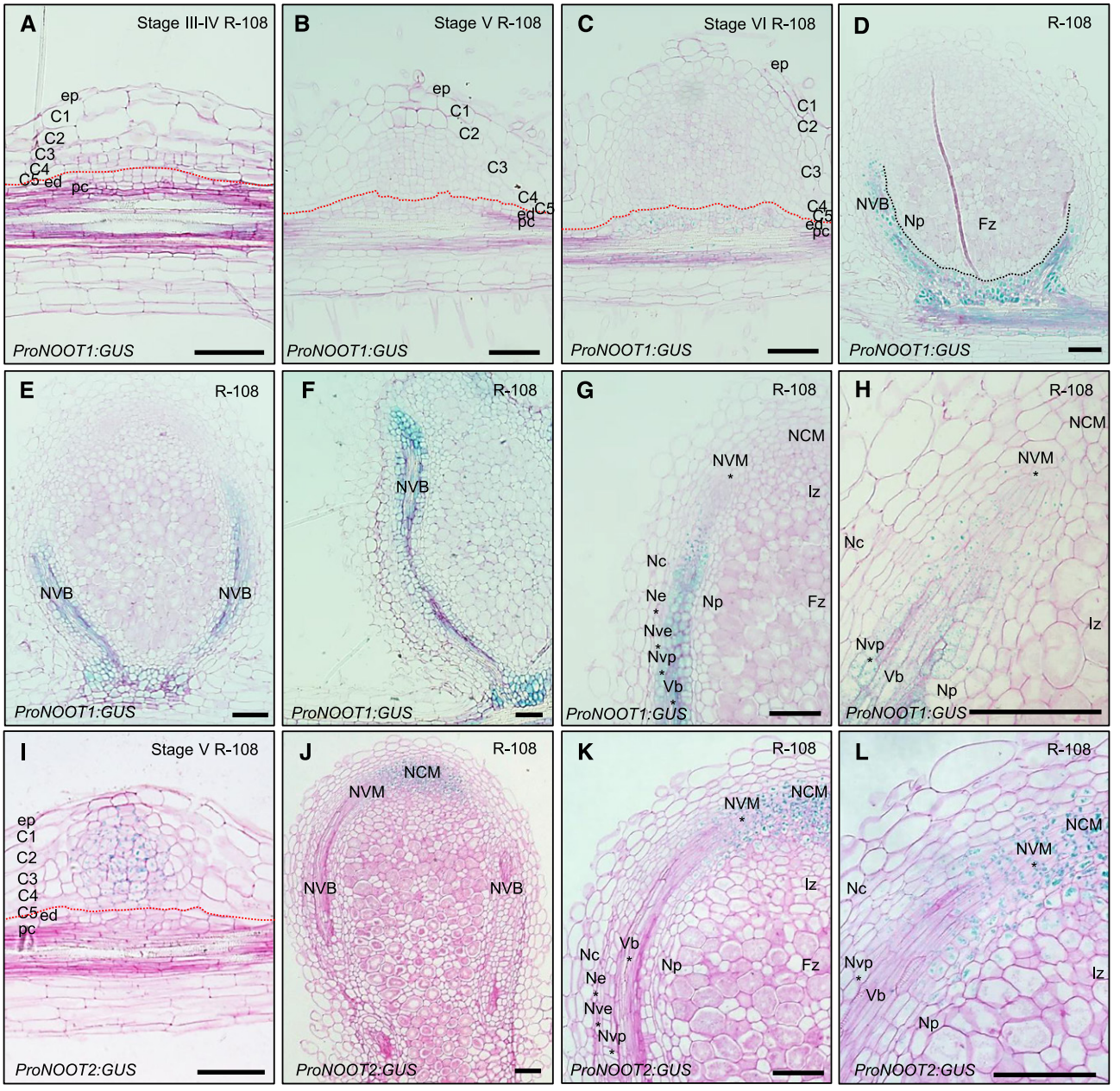

Figure 3. *ProNOOT1*:*GUS* and *ProNOOT2*:*GUS* expression patterns during R-108 nodule development. A to H, *ProNOOT1*:*GUS* expression pattern in nodule primordia and nodules of the R-108 stable transformant inoculated with WSM419. A, Stages III and IV nodule primordium with no *ProNOOT1*:*GUS* expression. B, Stage V nodule primordium with weak *ProNOOT1*:*GUS* expression in endodermis- and pericycle-derived cell layers. C, Stage VI nodule primordium showing *ProNOOT1*:*GUS* expression in endodermis- and pericycle-derived cell layers. D, An 8- to 9-dpi nodule showing *ProNOOT1*:*GUS* expression restricted in the basal part of the nodule and in the nodule vasculature. *ProNOOT1*:*GUS* is not expressed in adjacent nodule parenchyma tissues or in the nodule fixation zone. The black-dotted line separates the nodule parenchyma tissues and nodule fixation zone from the nodule vasculature. E and F, At later stages of nodule development, *ProNOOT1*:*GUS* continues to associate with the developing nodule vasculature. G, An 8- to 9-dpi nodule vascular bundle showing *ProNOOT1*:*GUS* expression in NVB cells. H, Magnification of G focusing on the junction between the NVM and NCM shows *ProNOOT1*:*GUS* expression in NVB vessel, pericycle, and endodermis cells. *ProNOOT1*:*GUS* expression is not observed in NCM. I to L, *ProNOOT2*:*GUS* expression in nodule primordia and mature nodules of *M. truncatula* Jemalong J5 transformed by hairy root and inoculated with WSM419. I, Stage V nodule primordium showing predominant *ProNOOT2*:*GUS* expression in C3/C4-derived cell layers and weak expression in C2- and C5-derived cell layers. J, Twelve- to 13-dpi nodule showing *ProNOOT2*:*GUS* expression in NCM. K, Magnification of J, showing *ProNOOT2*:*GUS* expression in NCM and in the apical NVB pericycle and endodermis cells. L, Magnification of K focusing on the junction between the NCM and NVM. C1, First cortex cell layer; C2, second cortex cell layer; C3, third cortex cell layer; C4, fourth cortex cell layer; C5, fifth cortex cell layer; ed, endodermis; ep, epidermis; Fz,

nodule vascular vessel, pericycle, and endodermis cells (Fig. 3, G and H). Furthermore, in situ RNA hybridization analyses using *MtNOOT1* antisense RNA probes confirmed *MtNOOT1* gene expression in the upper part of the NVBs and the absence of *MtNOOT1* transcripts in the NCM (Fig. 4, A and C; Supplemental Fig. S3).

The *MtNOOT1* gene expression pattern was clearly associated with NVB development, and it precisely defined the new territories derived from root pericycle and endodermis cells within the nodule.

MtNOOT2 Is Expressed in the NCM

To precisely define the spatial and temporal expression pattern of *MtNOOT2* during nodule development, we generated a *PromoterMtNOOT2*:*GUS* fusion (*ProNOOT2*:*GUS*). Similar expression patterns were obtained using both stable transgenic lines and transient hairy root transformed plants.

In stage V nodule primordium, *ProNOOT2*:*GUS* was expressed in dividing C3- and C4-derived cell layers (Fig. 3I). It should be noted that these C3-derived cells will become the NCM (Xiao et al., 2014). In nodules, *ProNOOT2*:*GUS* was expressed mostly in the NCM and extended toward the NVM, resulting in a star-like pattern (Fig. 3, J–L; Supplemental Fig. S2B).

Detailed histological analyses focusing on the NVM/NCM boundary region showed that *ProNOOT2*:*GUS* was associated with the NCM and extended to the apical nodule vascular pericycle and endodermis cells and to NVM surrounding cells (Fig. 3L). Furthermore, in situ RNA hybridization analysis using *MtNOOT2* antisense RNA probes confirmed *MtNOOT2* gene expression in the NCM and in the upper part of the NVBs (Fig. 4, B and D).

Taken together, our results show distinct *MtNOOT1* and *MtNOOT2* expression patterns that partially overlap at the NVM/NCM boundaries (Figs. 3 and 4). This expression pattern overlap suggests that MtNOOT1 and MtNOOT2 can interact together. Furthermore, this potential interaction is reinforced by yeast two-hybrid experiments showing a positive interaction between MtNOOT1 and MtNOOT2 (Supplemental Fig. S4).

The Loss of Function of *MtNOOT1* and *MtNOOT2* Triggers the Complete Loss of Nodule Identity and Leads to a Nonfixing Phenotype

To characterize the roles of *MtNOOT1* and *MtNOOT2* in nodule identity, we used two *Mtnoot1 Transposon of Nicotiana tabacum1* (*Tnt1*) insertional mutant lines, Tnk507 and NF2717, characterized previously as nodule homeotic mutants (Couzigou et al., 2012), as well as two *Mtnoot2 Tnt1* insertional mutant lines, NF5722 and NF5464 (Fig. 5A). In contrast to the *Mtnoot1* mutants, *Mtnoot2* NF5464 and NF5722 mutants did not exhibit any symbiotic phenotype. Thus, in order to investigate the consequences of a simultaneous *MtNOOT1* and *MtNOOT2* loss of function, *Mtnoot1 noot2* double mutants were made by crossing *Mtnoot1* NF2717 and *Mtnoot2* NF5464.

The impact of the *Mtnoot1*:*Tnt1* insertion (line Tnk507) and the *Mtnoot2*:*Tnt1* insertion (line NF5464) on the accumulation of *MtNOOT1* and *MtNOOT2* transcripts was measured by RT-qPCR in *Mtnoot1* and *Mtnoot2* single mutant nodules. *MtNOOT1* and *MtNOOT2* transcript levels were reduced drastically by 78% and 70% in their respective mutant backgrounds (Fig. 5B). Similarly, *MtNOOT1* and *MtNOOT2* transcript amounts measured by RT-qPCR in *Mtnoot1 noot2* double mutant nodules were reduced drastically by 90% and 76%, respectively. These results confirmed the knockout nature of these mutations (Fig. 5B).

M. truncatula R-108 inoculated with WSM419 formed unilobed nodules (55%) and multilobed nodules (45%; Fig. 6, A, B, and G). *Mtnoot1* inoculated with WSM419 formed four types of nodules: unilobed nodules (14%), multilobed nodules (35%), root-converted nodules (44%), and nodule-like structures (7%), which consist of successive nodule-to-root conversions coupled with rhizobia reinfection events generating complex and disorganized aggregates of nodule and root organs (Fig. 6G). *Mtnoot2* inoculated with WSM419 formed only unilobed nodules (52%) and multilobed nodules (48%), as observed in control R-108 plants (Fig. 6G). *Mtnoot1 noot2* inoculated with WSM419 formed few unilobed nodules (1%), few multilobed nodules (4%), and a majority of nodule-like structures (95%; Fig. 6, C–E and G). This severe and complete reversion of nodules into roots was observed in three independent *Mtnoot1 noot2* double mutant lines. The three independent *Mtnoot1 noot2* mutants also exhibited similar and important aerial modifications, but in this work, only the symbiotic aspects are described. *Mtnoot1 noot2* nodule-like structures presented often fasciated ectopic roots resulting in cryptic and unstable plurivascularized ectopic roots. These fasciated ectopic roots later dichotomized (Fig. 6, C and D). As observed already in *Mtnoot1*, *Mtnoot1 noot2* ectopic roots developed from the NVM and appeared to be functional, because nodule primordia could de novo initiate and give rise to new nodule like-structures (Fig. 6, D–F; Couzigou et al., 2012). This shows that the partially redundant *MtNOOT* genes are not essential for the recognition

Figure 3. (*Continued.*)
nodule fixation zone; Iz, infection zone; Nc, nodule cortex; Ne, nodule endodermis; Np, nodule parenchyma; Nve, nodule vascular endodermis; Nvp, nodule vascular pericycle; pc, pericycle; Vb, vascular bundle. In A, B, C, and I, nodule primordia were staged according to Xiao et al. (2014). Red-dotted lines indicate the boundaries between cortex-derived cell layers (above) and pericycle/endodermis-derived cell layers (below). Section thickness is 7 μm. Bars = 50 μm.

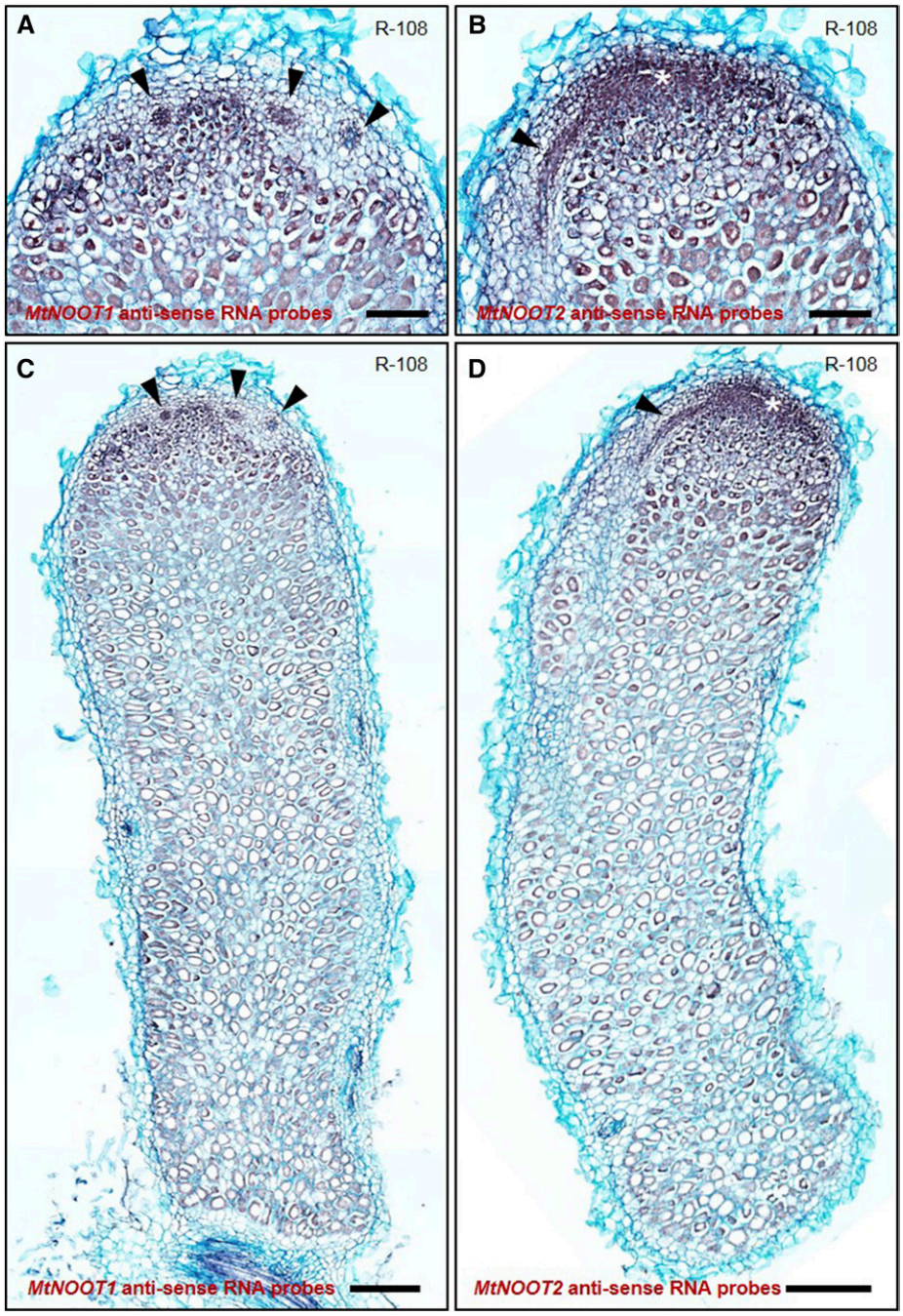

Figure 4. *MtNOOT1* and *MtNOOT2* in situ RNA hybridization expression patterns in R-108 nodules. In situ RNA hybridization was performed on longitudinal sections of a 28-dpi R-108 nodule inoculated with WSM419. A and C, Specific *MtNOOT1* transcript antisense RNA probes in nodule vascular bundle apex (black arrowheads). B and D, Specific *MtNOOT2* transcript antisense RNA probes in nodule central meristem (white asterisks) and in the upper part of nodule vascular bundles (black arrowheads). The R-108 nodule apices in A and B represent magnifications from the entire nodule images in C and D, respectively. For *MtNOOT1* and *MtNOOT2* in situ RNA hybridization, six and five nodules were sectioned, respectively. Section thickness is 12 µm. Bars = 50 µm (A and B) and 100 µm (C and D).

and infection processes but are essential for nodule development and identity.

The nitrogen fixation efficiency of R-108, *Mtnoot1*, *Mtnoot2*, and *Mtnoot1 noot2* whole nodule populations was assessed by acetylene reduction assays (Fig. 6H; Koch and Evans, 1966). The nitrogenase activities of *Mtnoot1* (15 nmol C_2H_4 h^{-1} $plant^{-1}$) and *Mtnoot2* (11 nmol C_2H_4 h^{-1} $plant^{-1}$) were not significantly different ($P = 0.32$ and

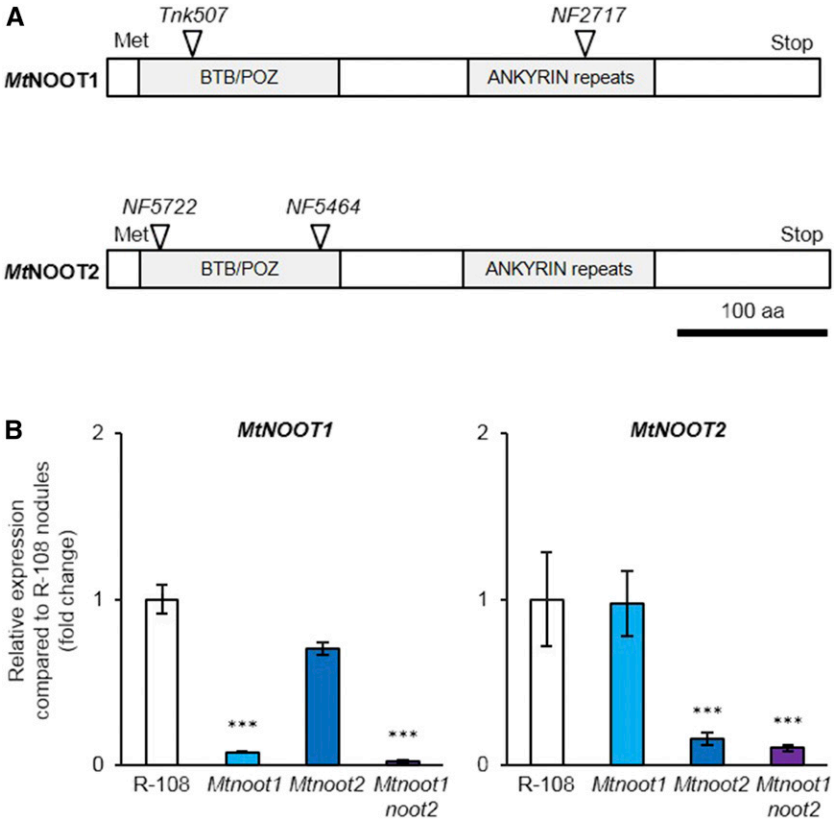

Figure 5. MtNOOT1 and MtNOOT2 *Tnt1* insertion positions and effects on *MtNOOT1* and *MtNOOT2* transcripts. A, Schemes of MtNOOT1 and MtNOOT2 protein structures containing BTB/POZ and ANKYRIN repeat domains. The positions of *Tnt1* insertions are indicated by triangles. aa, Amino acids. B, The effects of *Tnt1* insertions on *MtNOOT1* and *MtNOOT2* transcript accumulation were assessed by RT-qPCR in WSM419 inoculated nodules of *Mtnoot1* mutant (Tnk507; light blue bars), *Mtnoot2* mutant (NF5464; blue bars), and *Mtnoot1 noot2* (NF2717 × NF5464; purple bars) and compared with R-108 (white bars). Gene expression data represent relative expression normalized against the constitutively expressed *MtRRM* and *MtACT* reference genes and against R-108 nodules. Results represent means ± SE of two biological replicates (29 and 38 dpi) and two technical replicates. Asterisks indicate significant differences compared with the R-108 nodule (***, $P < 0.0001$, one-way ANOVA).

0.13, respectively; $\alpha = 0.01$) from R-108 nitrogenase activity (17 nmol C_2H_4 h^{-1} $plant^{-1}$). However, the *Mtnoot1 noot2* nitrogenase activity (0.3 nmol C_2H_4 h^{-1} $plant^{-1}$) was completely abolished ($P = 7.6 \times 10^{-10}$; $\alpha = 0.01$; Fig. 6H). This fix$^-$ phenotype was identical in our three independent *Mtnoot1 noot2* lines. In *Mtnoot1*, despite the presence of converted nodules, nitrogen fixation was not significantly different from that of R-108. The presence of lately converted and unconverted functional nodules in *Mtnoot1* probably compensated for the partial nodule loss of identity (Fig. 6, G and H).

These results indicate that the loss of function of the two MtNOOT genes triggers a complete loss of nodule identity, subsequently leading to nitrogen fixation failure. Thus, *MtNOOT* genes are redundant for nodule identity maintenance and are essential to guarantee an efficient and sustainable symbiotic process.

Bacterial Accommodation Is Nodule Identity Dependent

To better understand why *Mtnoot1 noot2* was fix$^-$, we analyzed bacterial occupancy in R-108, *Mtnoot1*, *Mtnoot2*, and *Mtnoot1 noot2* nodules using WSM419 expressing the enhanced GFP (eGFP; Fig. 7). R-108 and *Mtnoot2* nodules were highly colonized by rhizobia (Fig. 7, A, E, I and C, G, K); however, *Mtnoot1* and *Mtnoot1 noot2* early converted nodules showed a reduced level of occupancy by rhizobia (Fig. 7, B, F, J and D, H, L). Histological analyses of R-108, *Mtnoot1*, *Mtnoot2*, and *Mtnoot1 noot2* nodules using Technovit sections showed similar results: R-108 and *Mtnoot2* nodules were highly colonized by rhizobia (Fig. 7, M and O), while *Mtnoot1* and *Mtnoot1 noot2* converted nodules showed low rhizobia colonization and mostly collapsed infected cells (Fig. 7, N and P). These results explain the fix$^-$ phenotype of *Mtnoot1 noot2*, showing only converted nodules that are converted precociously as compared with *Mtnoot1*. This suggests that nodule identity maintenance is a prerequisite to host symbiotic rhizobia within the nodule and that *Mtnoot1* and *Mtnoot1 noot2* converted nodules might trigger defense reactions following bacterial infection.

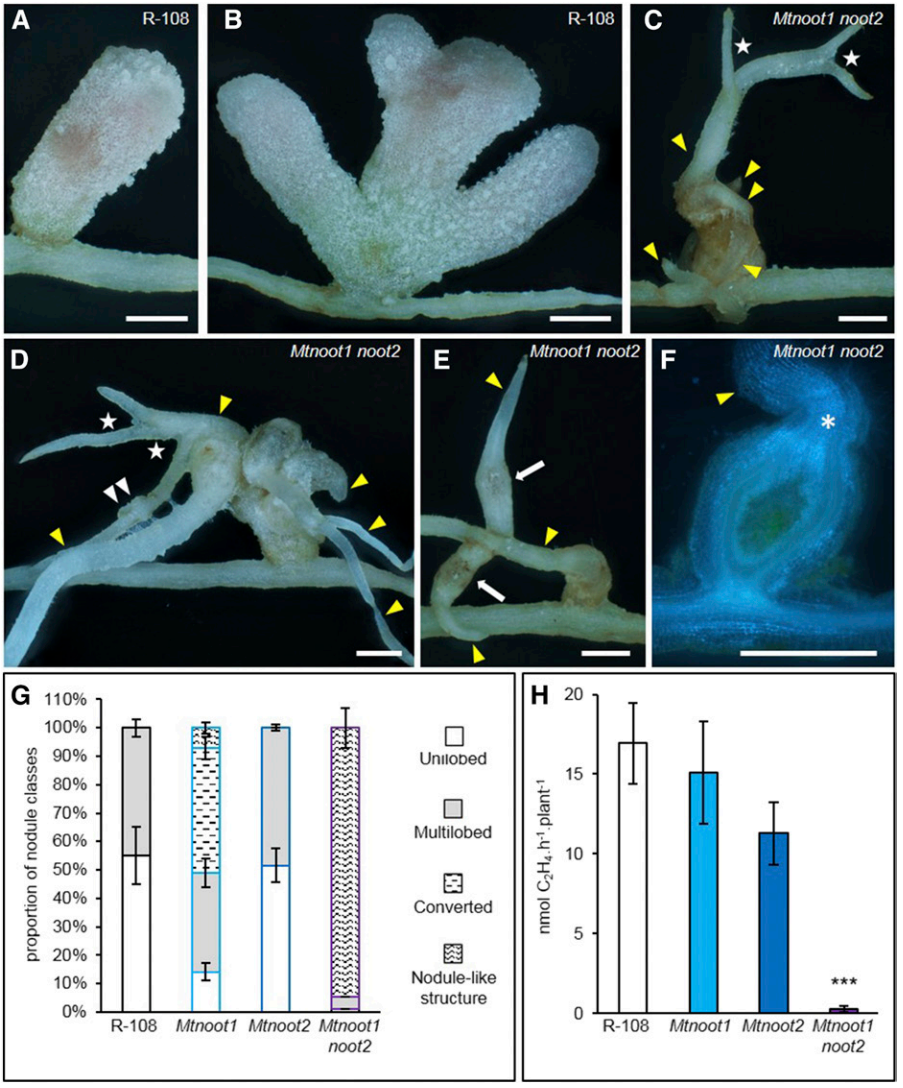

Figure 6. *Mtnoot1 noot2* full loss of nodule identity and fix⁻ phenotype. A to E, Nodules inoculated with WSM419 35 dpi. A, R-108 unilobed nodule. B, R-108 multilobed nodule. C to E, *Mtnoot1 noot2* complete nodule-to-root homeosis. F, Longitudinal section of a 32-dpi *Mtnoot1 noot2* nodule inoculated with WSM419 showing the continuum between nodule vascular bundles and ectopic root vasculatures (white asterisk). In C to F, yellow arrowheads indicate cryptic roots emerging from *Mtnoot1 noot2* nodules, stars indicate plurivascularized ectopic root dichotomies, white arrowheads indicate nodule primordia formation on nodule ectopic root, and white arrows indicate secondary nodule-to-root homeosis on nodule ectopic root. G, *Mtnoot* nodule phenotypes. Wild-type unilobed nodules (white bars), wild-type multilobed nodules (gray bars), nodule-to-root conversions (dashed bars), and nodule-like structure (wave bars) are represented. H, *Mtnoot* nitrogen fixation efficiencies. R-108 (white bar), *Mtnoot1* (light blue bar), *Mtnoot2* (blue bar), and *Mtnoot1 noot2* (purple bar) are represented. Asterisks indicate a significant difference relative to R-108 (***, $P < 0.001$, Mann-Whitney test). Results in G and H represent means ± SE of three independent biological experiments containing nine plants each (27 plants analyzed for each genotype). The number of nodules analyzed is as follows: R-108, 205; *Mtnoot1*, 141; *Mtnoot2*, 153; *Mtnoot1 noot2*, 94. Section thickness in F is 60 µm. Bars in A to F = 1 mm.

Mtnoot1 noot2 Inoculated with Infection-Deficient Rhizobia Forms Ectopic Roots from Aborted Nodule Primordia

Surface polysaccharide mutants often are deficient in infection (inf⁻) and induce fix⁻ nodule primordia-like structures arrested early in nodule organogenesis. In agreement with previous studies (Putnoky et al., 1990), R-108 inoculated with *Sinorhizobium meliloti* Rm41 (Rm41), Rm41 *kps*⁻, or Rm41 *exo*⁻ formed wild-type nodules (Supplemental Fig. S5, A–C and E–G), in contrast to R-108 inoculated with Rm41 *exo*⁻ *kps*⁻, which formed arrested and inf⁻ nodule primordia (Supplemental Fig. S5, D and H). To better understand at which stages of nodule development *MtNOOT1* and *MtNOOT2* act, we studied the nodule

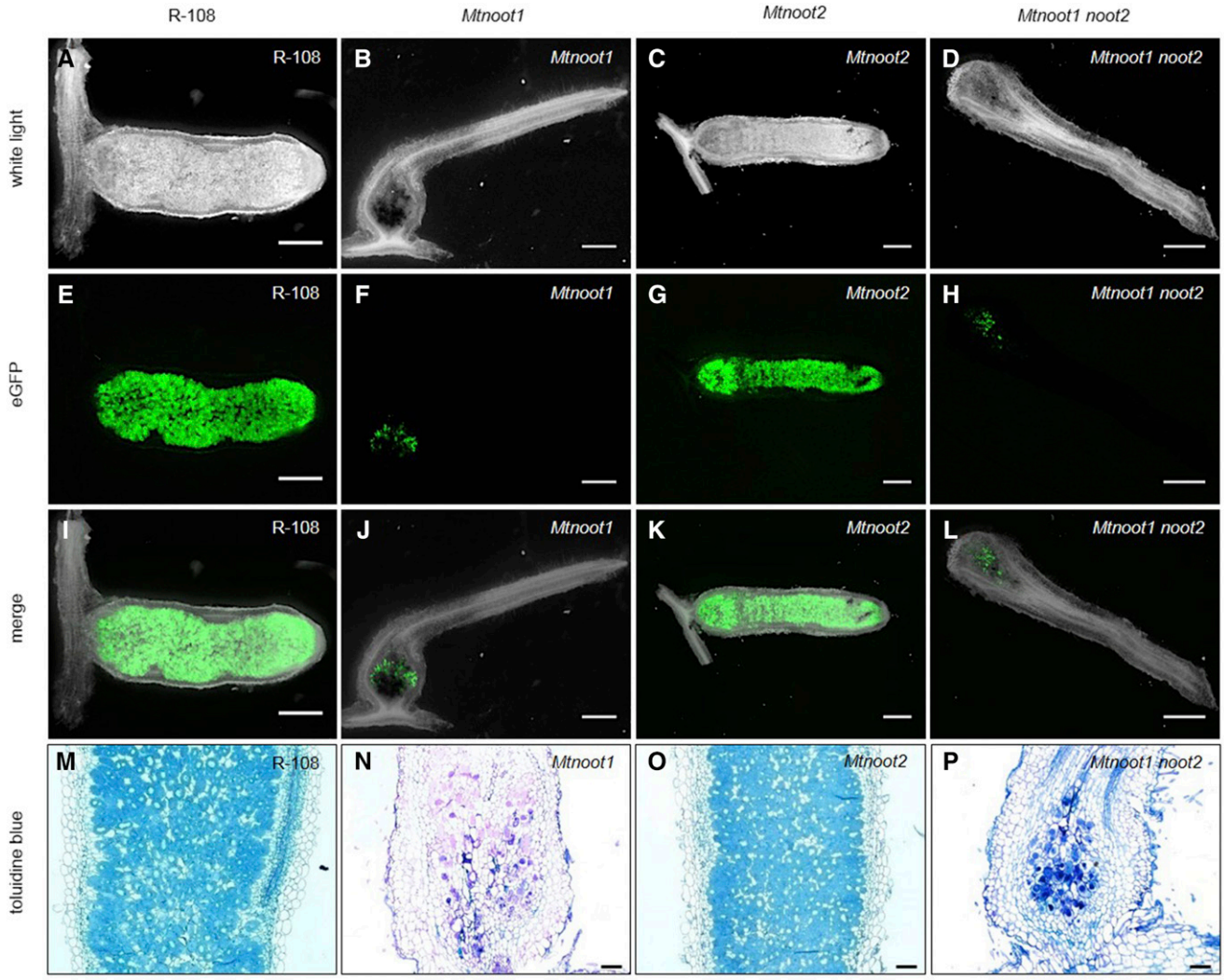

Figure 7. *Mtnoot1* and *Mtnoot1 noot2* early converted nodules are altered in bacterial hosting. A to L, Semithin sections of R-108, *Mtnoot1*, *Mtnoot2*, and *Mtnoot1 noot2* nodules at 42 dpi with WSM419 eGFP. A to D, White light. E to H, UV light showing eGFP. I to L, Merge of white light and UV light images. M to P, Technovit sections stained with Toluidine Blue of R-108, *Mtnoot1*, *Mtnoot2*, and *Mtnoot1 noot2* nodules at 35 dpi with WSM419. *Mtnoot1* and *Mtnoot1 noot2* nodules are poorly colonized by rhizobia (B, F, J, N and D, H, L, P, respectively) compared with R-108 and *Mtnoot2* nodules (A, E, I, M and C, G, K, O, respectively). The number of nodules sectioned and imaged for the eGFP rhizobia localization experiment is as follows: R-108, 26; *Mtnoot1*, 10; *Mtnoot2*, 14; *Mtnoot1 noot2*, 28. Section thickness is 60 µm (A–L) and 5 µm (M–P). Bars = 500 µm (A–L) and 50 µm (M–P).

phenotype of *Mtnoot1 noot2* inoculated with this inf$^-$ rhizobium mutant. *Mtnoot1 noot2* inoculated with Rm41, Rm41 *kps*$^-$, or Rm41 *exo*$^-$ formed converted nodules, as expected (Supplemental Fig. S5, I–K and M–O); however, *Mtnoot1 noot2* inoculated with Rm41 *exo*$^-$ *kps*$^-$ formed ectopic roots originating from inf$^-$ nodule primordia (Supplemental Fig. S5, L and P).

These results suggest that Rm41 *exo*$^-$ *kps*$^-$ aborted nodule primordia cannot develop into functional nodules, but they can still form nodule ectopic roots in the *Mtnoot1 noot2* mutant. This shows that nodule-to-root conversion can occur before the acquisition of the different zones of the indeterminate nodule, independently of rhizobial nodule colonization.

ProMtNOOT2:GUS and *ProMtNOOT1:GUS* Gene Expression Patterns Are Modified in *Mtnoot1* and *Mtnoot2* Backgrounds, Respectively

To better understand the relationship between *MtNOOT1* and *MtNOOT2*, we studied their expression patterns in opposite mutant backgrounds. For this, we generated stable *Mtnoot1* and *Mtnoot2* transgenic plants

expressing *ProNOOT2*:*GUS* and *ProNOOT1*:*GUS*, respectively.

In *Mtnoot1* stage V nodule primordium, *ProNOOT2*:*GUS* expression was detected in dividing cells derived from root C3, C4, and C5 as in R-108. In addition, *ProNOOT2*:*GUS* expression also was detected in dividing cells derived from the root pericycle and endodermis corresponding to the *MtNOOT1* expression domain (Fig. 8, A and C). In R-108 and *Mtnoot1* unconverted nodules, *ProNOOT2*:*GUS* was expressed in the NCM (Supplemental Fig. S6, A and B). In converting *Mtnoot1* nodules, *ProNOOT2*:*GUS* expression was conserved in the NCM, and it was never observed in emerging ectopic roots (Supplemental Fig. S6, C and D). Once *Mtnoot1* nodules were fully converted, dividing NCM cells were not found and NCM-associated *ProNOOT2*:*GUS* expression was completely lost (Fig. 8E; Supplemental Fig. S6, D and E). Interestingly, nodule primordia developing from *Mtnoot1* nodule ectopic roots correctly expressed *ProNOOT2*:*GUS* (Supplemental Fig. S6E).

These results suggest that, in *Mtnoot1* converted nodules, the NCM ceased to function and *MtNOOT2* was no longer expressed in NCM. Thus, *MtNOOT2* gene expression is dependent on the nodule identity integrity conferred by *MtNOOT1*.

As in R-108, in *Mtnoot2* nodules, *ProNOOT1*:*GUS* was expressed in NVB and NVM (Fig. 8, B and F). However, in *Mtnoot2* nodules, additional *ProNOOT1*:*GUS* expression was detected in the dividing cells of the NCM. This suggests that, in *Mtnoot2*, the *MtNOOT1* expression domain is extended to the NCM and might compensate for the loss of function of *MtNOOT2*. These results might explain the absence of a symbiotic phenotype in *Mtnoot2*.

Nodule Homeosis Is Accompanied by RAM, Defense, and Symbiotic Marker Gene Expression Changes

To better understand the molecular changes occurring during the nodule-to-root homeosis, we analyzed the transcript levels of RAM, defense, and symbiotic markers in R-108, *Mtnoot1*, *Mtnoot2*, and *Mtnoot1 noot2* nodules.

MtCRINKLY4 (MtACR4) is a receptor-kinase ortholog to AtCRINKLY4 known to control the activity of AtWOX5 via the perception of CLAVATA3/ENDOSPERM SURROUNDING REGION-related AtCLE40 peptides in Arabidopsis (Stahl et al., 2009; Roux et al., 2014). MtSHORT ROOT (MtSHR) is a GIBBERELLIC-ACID INSENSITIVE (GAI), REPRESSOR of GAI (RGA), and SCARECROW family TF ortholog to AtSHORT ROOT required for stem cell maintenance in Arabidopsis (Levesque et al., 2006; Cui et al., 2007). MtPLT2 is an AP2/ERF TF ortholog to AtPLETHORA that is involved in auxin-mediated positive regulation of cell division and proliferation during root development in Arabidopsis (Aida et al., 2004; Mähönen et al., 2014). In *M. truncatula* nodules, *MtPLT2* is expressed predominantly in the NVM (Roux et al., 2014; Franssen et al., 2015).

In *Mtnoot1* and *Mtnoot1 noot2* nodules, the RAM marker genes *MtACR4*, *MtSHR*, and *MtPLT2* were up-regulated relative to R-108 nodules (Fig. 9A). In *Mtnoot2* nodules, the expression of RAM marker gene expression was not significantly different from that in R-108 (Fig. 9A). In R-108, gene expression kinetics showed that *MtPLT1* to *MtPLT4* were induced in the RAM and in nodules relative to noninoculated roots. *MtPLT3/MtPLT4* were more expressed in nodules than in the RAM, while *MtPLT1/MtPLT2* were less expressed in nodules compared with the RAM (Supplemental Fig. S7A). In R-108, the *MtPLT2* gene was expressed at a low level. However, in *Mtnoot1* and *Mtnoot1 noot2* nodules, *MtPLT2* gene expression was strongly up-regulated as in R-108 RAM (Fig. 9A; Supplemental Fig. S7, A and B). The expression of *MtPLT1*, *MtPLT3*, and *MtPLT4* in *Mtnoot* mutant nodules was more variable and difficult to interpret (Supplemental Fig. S7B). The up-regulation of RAM markers such as *MtACR4*, *MtSHR*, and *MtPLT2* is in agreement with the nodule-to-root identity shift occurring in *Mtnoot1* and *Mtnoot1 noot2* nodules.

The defense-related *MtPHENYLALANINE AMMONIA LYASE2* (*MtPAL2*), *MtPR10*, and *MtNON-DISEASE RESISTANCE1-LIKE* (*MtNDR1-LIKE*) genes are normally repressed in R-108 nodules to allow bacterial colonization (Bourcy et al., 2013b; Berrabah et al., 2015). In *Mtnoot1* and *Mtnoot1 noot2* nodules, these defense-related marker genes were up-regulated relative to R-108 nodules. In *Mtnoot2* nodules, defense-related marker gene expression was not significantly different from that in R-108 (*MtPAL2*, *MtPR10*, and *MtNDR1-LIKE*, $P = 0.1$, 0.09, and 0.75, respectively; $\alpha = 0.01$; Fig. 9B).

In parallel to RAM and defense-like marker gene expression, we also analyzed transcript levels of symbiotic genes. *MtCYTOKININ RESPONSE1* (*MtCRE1*) is a cytokinin receptor essential for the symbiotic interaction (Gonzalez-Rizzo et al., 2006; Plet et al., 2011), and *MtNIN* is a master symbiotic regulator. The transcript amounts of *MtCRE1* and *MtNIN* were not significantly affected in the single mutants (*MtCRE1*, $P = 0.27$ and 0.03; *MtNIN*, $P = 0.013$ and 0.12, in *Mtnoot1* and *Mtnoot2*, respectively; $\alpha = 0.01$), but their expression appeared to be reduced in *Mtnoot1 noot2* nodules (Fig. 9C). *MtNCR001* encodes a nodule-specific Cys-rich peptide that is expressed during the later stages of nodulation, *MtLEGH1* is essential for oxygen transport in nodules, and *MtDOES NOT FIX2* (*MtDNF2*) and *MtSymbiotic CYSTEINE-RICH RECEPTOR KINASE-LIKE* (*MtSymCRK*) are essential nodule-specific genes repressing immunity after rhizobia internalization (Bourcy et al., 2013a, 2013b; Berrabah et al., 2014a, 2014b, 2015, 2018). The transcript levels of these symbiotic genes were reduced significantly in *Mtnoot1* ($P = 6.5 \times 10^{-5}$, 1.1×10^{-3}, 3.3×10^{-2}, and 4×10^{-3}, respectively; $\alpha = 0.01$), not affected significantly in *Mtnoot2* ($P = 0.11$, 0.56, 0.95, and 0.19, respectively; $\alpha = 0.01$), and reduced significantly in *Mtnoot1 noot2* relative to R-108 ($P = 2.2 \times 10^{-7}$, 2.5×10^{-6}, 3×10^{-3}, and 9.9×10^{-5}, respectively; $\alpha = 0.01$; Fig. 9C).

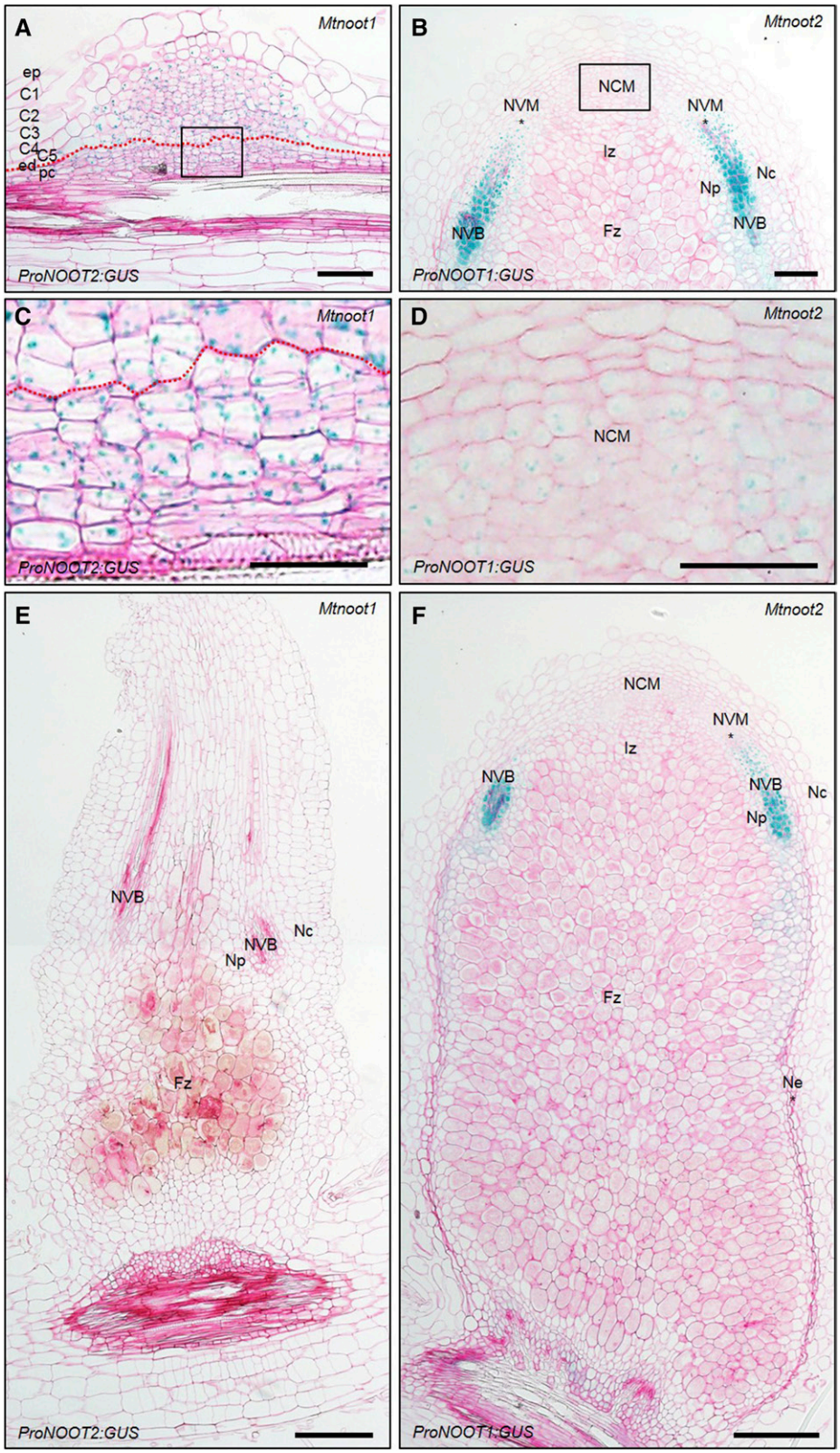

Figure 8. Expression patterns of *ProNOOT2*:*GUS* in *Mtnoot1* and *ProNOOT1*:*GUS* in *Mtnoot2*. A, C, and E, *ProNOOT2*:*GUS* expression pattern in nodule primordium and nodule of an *Mtnoot1* stable transformant inoculated with WSM419. A, *Mtnoot1* stage V nodule primordium showing *ProNOOT2*:*GUS* expression in dividing cells derived from C3, C4, and C5 cell layers and ectopic expression of *ProNOOT2*:*GUS* in dividing cells derived from pericycle and endodermis. The black frame indicates

The reduced expression of *MtDNF2* and *MtSymCRK* is in agreement with the observed up-regulation of defense-related genes (Fig. 9B), the presence of collapsed infected cells (Fig. 7, M–P), and the poor rhizobia colonization observed in *Mtnoot1* and *Mtnoot1 noot2* nodules (Fig. 7, A–L). Furthermore, these results associate with the accumulation of the defense phytohormone salicylic acid in *Mtnoot1* nodules (Supplemental Fig. S8).

These results demonstrate that the loss of nodule identity is accompanied by the up-regulation of RAM and defense gene markers as well as by the down-regulation of symbiotic gene markers. These changes occur in *Mtnoot1* and *Mtnoot1 noot2* nodules but are more important in the *Mtnoot1 noot2* double mutant.

The Class II *MtKNOTTED1-LIKE HOMEOBOX9* Gene Expression Pattern Is *Mtnoot1* Dependent

In Arabidopsis meristem-to-organ-boundaries and at the base of lateral organs, AtBOPs repress cell proliferation via the repression of class I KNOTTED1-LIKE HOMEOBOX (KNOX) TFs (Ha et al., 2003, 2004; Žádníková and Simon, 2014). KNOX TFs contain homeodomains and belong to the THREE AMINO ACID LOOP EXTENSION family. While class I KNOX TFs are required for organ initiation and patterning, as well as for meristem establishment and maintenance, the roles of class II KNOX TFs are less understood (Hake et al., 2004; Hay and Tsiantis, 2010). However, in Arabidopsis, class II KNOX TFs appear to function antagonistically with class I KNOX TFs (Furumizu et al., 2015).

In *M. truncatula*, class II *MtKNOX3*, *MtKNOX5*, and *MtKNOX9* are constitutively expressed in the root stele, including the pericycle and endodermis, and are up-regulated in nodules (Azarakhsh et al., 2015; Di Giacomo et al., 2016). In *M. truncatula* nodules, *MtKNOX9* expression is associated with the NM (Di Giacomo et al., 2016).

In R-108, *Mtnoot1*, and *Mtnoot1 noot2* nodules, the expression pattern of *MtKNOX9* was determined using a *PromoterMtKNOX9:GUS:terminatorMtKNOX9* (*ProKNOX9:GUS*) fusion. In R-108 nodules, *ProKNOX9:GUS* was expressed in the NM and the root stele, while weaker signals were observed in the NVB (Fig. 10A). However, in *Mtnoot1* and *Mtnoot1 noot2* converted nodules, *ProKNOX9:GUS* expression in the NM was lost and delocalized completely to the NVB and ectopic root vasculature (Fig. 10, B and C).

RT-qPCR analysis confirmed that *MtKNOX9* behaves as a symbiotic gene because its transcripts were significantly down-regulated in *Mtnoot1* and *Mtnoot1 noot2* nodules relative to R-108 nodules ($P = 2.4 \times 10^{-2}$ and 4.8×10^{-2}, respectively; $\alpha = 0.05$). Such down-regulation could reflect the loss of *ProKNOX9:GUS* expression in the NM (Supplemental Fig. S9). Similarly, *MtKNOX3* expression also was down-regulated in *Mtnoot1* and *Mtnoot1 noot2* nodules; however, *MtKNOX5* expression followed the opposite pattern and was induced in *Mtnoot1* and *Mtnoot1 noot2* nodules (Supplemental Fig. S9).

These results show that, once nodule identity is lost, NCM-associated *ProKNOX9:GUS* expression also is lost and that *MtKNOX9* acquires a root-like expression pattern associated with the vascular tissues (Di Giacomo et al., 2016).

DISCUSSION

Legume Plants Retained Two Distinct *NBCL* Genes Sharing a Redundant Function in Nodule Identity

In the Papilionaceae subfamily, except for *L. japonicus* from the Loteae tribe (Magne et al., 2018), species from the Fabeae, Cicereae, Phaseoleae, and Genisteae tribes possess at least two distinct *NBCL* paralogs that were probably present in legume ancestors. A more extensive analysis of nodulating species will clarify if this dual NBCL subclade model represents a general feature for legume species able to establish symbiosis with N_2-fixing bacteria.

In this study, we first further characterized the expression of the *M. truncatula MtNOOT1* gene belonging to the legume-specific *NBCL1* subclade. In agreement with the literature, *MtNOOT1* was constitutively

Figure 8. (*Continued.*)
the magnified zone shown in C. The nodule primordium was staged according to Xiao et al. (2014). C, Magnification of the boundary (red-dotted line) between cortex-derived cell layers (above) and pericycle/endodermis-derived cell layers (below) in *Mtnoot1* primordium showing the ectopic expression of *ProNOOT2*:*GUS* in pericycle/endodermis-derived cell layers. E, Entire 21-dpi *Mtnoot1* converted nodule showing the complete loss of NCM cells and of the NCM-associated *ProNOOT2*:*GUS* expression pattern. Nodule zone organization is lost, and the nodule endodermis cell layer is not established. B, D, and F, *ProNOOT1*:*GUS* expression pattern in nodules of an *Mtnoot2* stable transformant inoculated with *S. medicae* WSM419. B, *Mtnoot2* nodule apical zone showing the *ProNOOT1*:*GUS* expression pattern in the upper part of the nodule vasculature and in NVM 21 dpi. The black frame indicates the magnified zone shown in D. D, Magnification of *Mtnoot2* NCM showing dividing cells with faint ectopic expression of *ProNOOT1*:*GUS*. F, Entire 21-dpi *Mtnoot2* nodule showing wild-type nodule zone organization and the *ProNOOT1*:*GUS* expression pattern in the upper part of the nodule vasculature and in NVM. The faint expression of *ProNOOT1*:*GUS* in NCM is not visible at this magnification level. C1, First cortex cell layer; C2, second cortex cell layer; C3, third cortex cell layer; C4, fourth cortex cell layer; C5, fifth cortex cell layer; ed, endodermis; ep, epidermis; Fz, nodule fixation zone; Iz, infection zone; Nc, nodule cortex; NCM, nodule central meristem; Ne, nodule endodermis; Np, nodule parenchyma; NVB, nodule vascular bundle; NVM, nodule vascular meristem; pc, pericycle. Section thickness is 7 µm. Bars = 50 µm (A and B), 25 µm (C and D), and 100 µm (E and F).

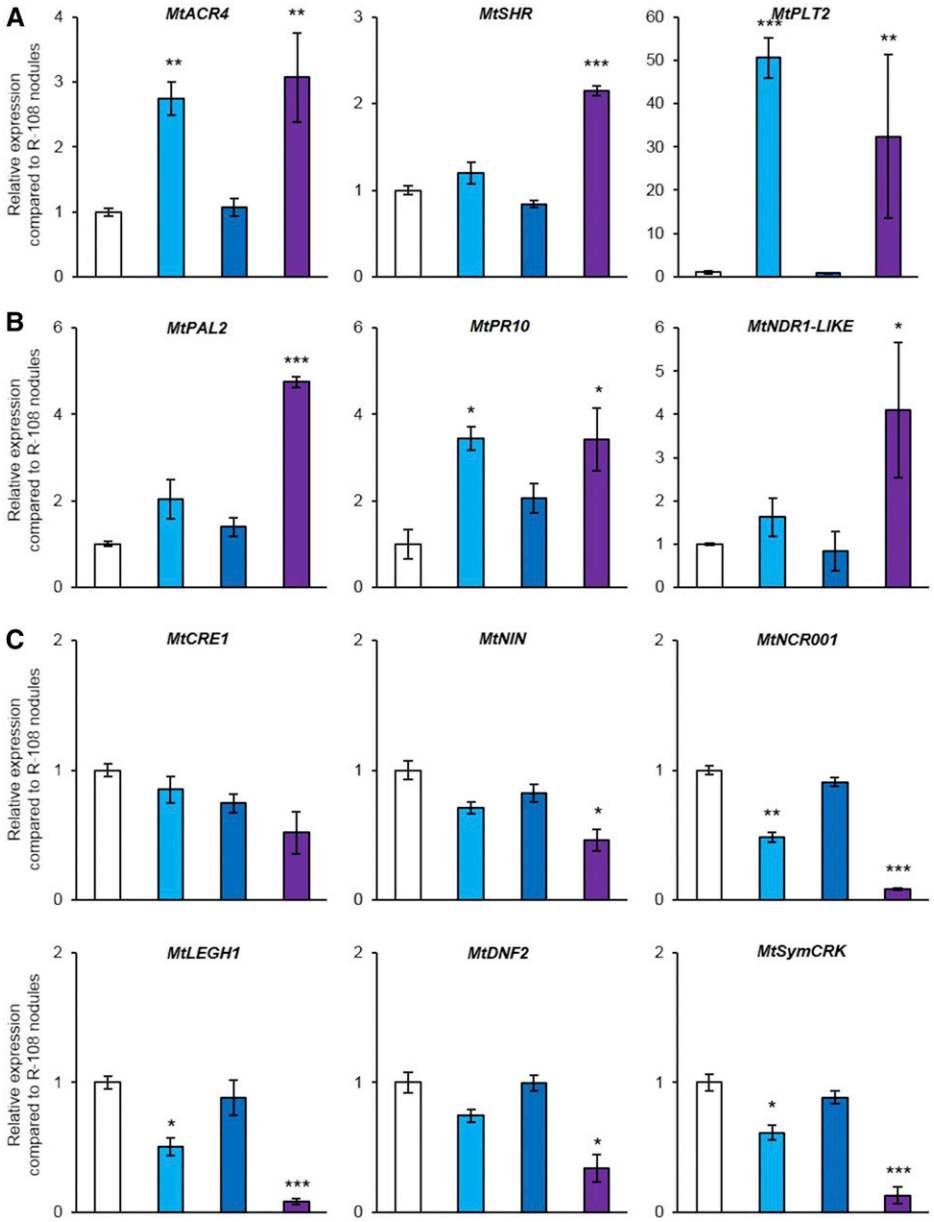

Figure 9. *Mtnoot1* and *Mtnoot1 noot2* nodule homeosis is associated with RAM, defense, and symbiotic marker gene expression changes. RT-qPCR gene expression analysis is shown in WSM419 inoculated nodules of *Mtnoot1* (light blue bars), *Mtnoot2* (blue bars), and *Mtnoot1 noot2* (purple bars) relative to R-108 (white bars). A, *MtACR4*, *MtSHR*, and *MtPLT2* RAM marker gene expression. B, *MtPAL2*, *MtPR10*, and *MtNDR1-LIKE* defense marker gene expression. C, *MtCRE1*, *MtNIN*, *MtNCR001*, *MtLEGH1*, *MtDNF2*, and *MtSymCRK* symbiotic marker gene expression. The expression of various marker genes is modified significantly in *Mtnoot1* and *Mtnoot1 noot2* mutants showing nodule-to-root homeosis, while it is not modified significantly in the *Mtnoot2* mutant. Gene expression data represent relative expression normalized against the constitutively expressed *MtRRM* and *MtACT* reference genes and against R-108 nodules. Results represent means ± SE of two biological replicates (29 and 38 dpi) and two technical replicates. Asterisks indicate significant differences relative to the R-108 nodule (*, $P < 0.01$; **, $P < 0.001$; and ***, $P < 0.0001$, one-way ANOVA).

expressed in roots and induced in nodules (Couzigou et al., 2012). In addition, in accordance with transcriptomic data showing the early repression of *MtNOOT1* in roots following Nod factor treatment (Herrbach et al., 2017), we found that *MtNOOT1* expression was down-regulated at the beginning of symbiosis and that *ProNOOT1:GUS* expression was absent during early nodule primordium stages. These results suggest that *MtNOOT1* expression is repressed at the beginning of nodule establishment to allow the development of new vascular domains derived from the root vasculature. At late primordia developmental stages, *MtNOOT1*

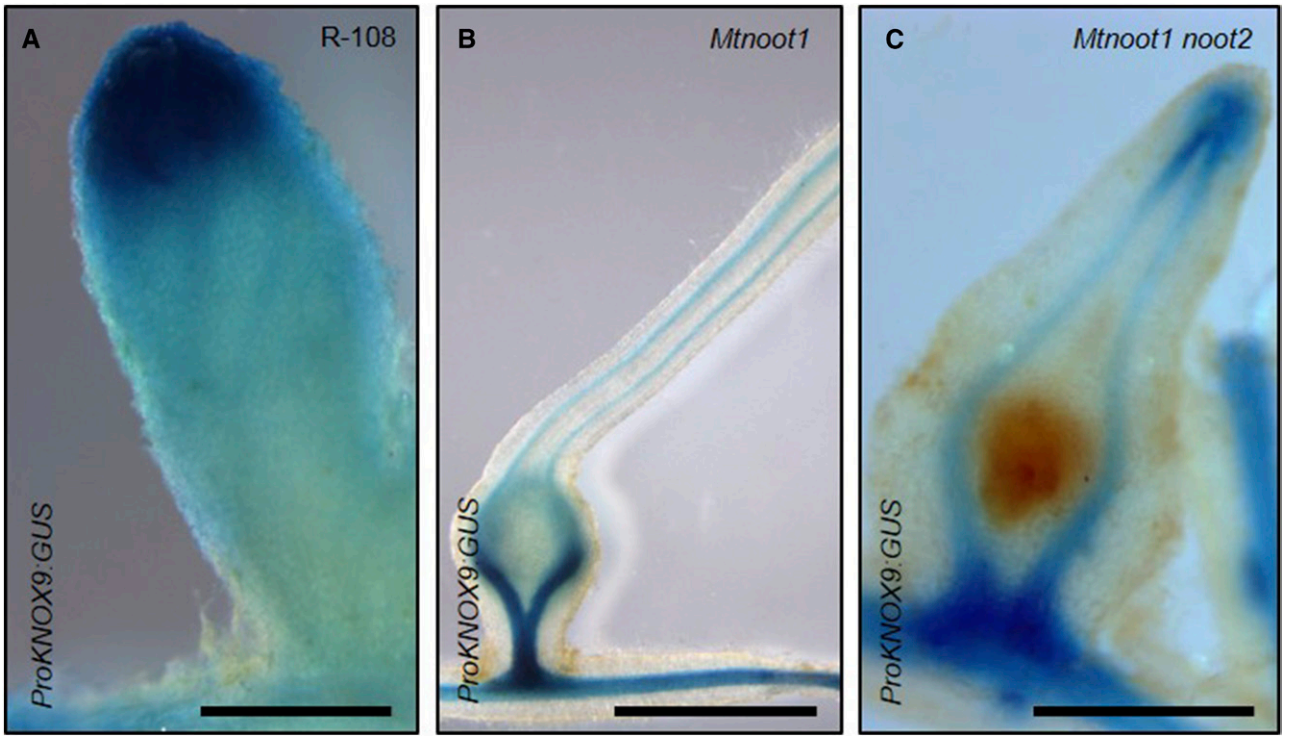

Figure 10. *ProKNOX9:GUS* expression pattern changes during *Mtnoot1* and *Mtnoot1 noot2* nodule homeosis. The *ProKNOX-9:GUS* expression pattern is shown in 35-dpi R-108, *Mtnoot1*, and *Mtnoot1 noot2* nodules inoculated with *S. meliloti*. A, R-108 nodules showing *ProKNOX9:GUS* expression mostly in the apical part of the nodule, with weak expression along the NVB and expression in the root central cylinder. B and C, *Mtnoot1* and *Mtnoot1 noot2* converted nodules showing the complete loss of NCM-associated *ProKNOX9:GUS* expression and the *ProKNOX9:GUS* expression shifts toward the NVB and the ectopic root vasculature. Bars = 500 µm (A and C) and 1 mm (B).

gene expression was induced and *ProNOOT1:GUS* expression was associated with NVB tissues derived from the root pericycle/endodermis cell layers. This suggests that, once NVBs are established, *MtNOOT1* is reactivated to control the growth and to define the territory of the NVB inside the nodule.

In addition to *MtNOOT1*, we characterized the expression of its paralog, *MtNOOT2*, belonging to the legume-specific NBCL2 subclade. *MtNOOT2* was not expressed in roots but it was induced early in nodule primordia. In *P. sativum*, *PsCOCH2* is orthologous to *MtNOOT2*, and *P. sativum* expression data supported our results, since *MtNOOT2* and *PsCOCH2* expression behaved similarly. Using a *ProNOOT2:GUS* fusion, we showed that *MtNOOT2* was expressed early in the pre-NCM (C3 dividing cells) in the nodule primordium and in both the NCM and NVM of mature nodules. Furthermore, we demonstrated that *MtNOOT2* behaved as a symbiotic gene and that its gene expression kinetic was similar to that of *MtNIN*. Based on these findings, it would be interesting to study the eventual relationships between *MtNOOT2*, *MtNIN*, and/or *MtNIN* downstream targets. In particular, the *MtNUCLEAR FACTOR-YA1* subunit gene (formerly called *MtHAEM ADHESION PROTEIN2-1*) is a downstream target of *MtNIN* encoding a CCAAT box-binding TF that is required for NM establishment, functioning, and persistence (Combier et al., 2006, 2008; Soyano et al., 2013; Laporte et al., 2014).

In this work, we demonstrate that *MtNOOT1* and *MtNOOT2* have distinct gene expression patterns overlapping at the NCM/NVM junctions. In addition, we show that MtNOOT1 and MtNOOT2 can form homodimers and heterodimers in yeast. Such interactions between BTB/POZ and ANKYRIN repeat-containing proteins are common and have been described previously in the literature (Mou et al., 2003; Hepworth et al., 2005). Our results suggest that MtNOOT1 and MtNOOT2 proteins interact at the NCM/NVM boundaries to coordinate NCM and NVM meristematic subdomain activities and to regulate the indeterminate nodule identity.

The *ProNOOT1:GUS* and *ProNOOT2:GUS* expression patterns in *Mtnoot2* and *Mtnoot1* plants, respectively, provide additional clues for understanding the functions of MtNOOTs. Our results suggest that MtNOOT1 might inhibit the expression of *MtNOOT2* in its own expression domain (pericycle- and endodermis-derived cell layers). In addition, the conservation of NCM identity and activity, as well as NCM-associated *MtNOOT2* expression, are clearly dependent on the nodule identity conferred by *Mt*NOOT1. Thus, *Mt*NOOT1 is

required for repressing NVM activity but also to maintain NCM activity.

Moreover, in *Mtnoot2*, the *ProNOOT1:GUS* fusion was ectopically detected in the NCM. This suggests that MtNOOT1 can complement the loss of function of *MtNOOT2*. The complementation of *Mt*NOOT2 function by *Mt*NOOT1 could explain the absence of a nodule phenotype in *Mtnoot2*.

Our results show that *MtNOOT1* and *MtNOOT2* have precise expression domains, and this suggests that a strict definition of the nodule territories is a prerequisite for nodule identity establishment and maintenance.

The Nodule-to-Root Identity Shift

In *Mtnoot1 noot2*, the loss of nodule identity is increased relative to *Mtnoot1*. The loss of function of *MtNOOT1* and *MtNOOT2* triggers earlier nodule-to-root conversions and impacts almost all *M. truncatula* nodules. This indicates that *Mt*NOOT1 and *Mt*NOOT2 have complementary but partially redundant functions for nodule development and nodule identity. In *Mtnoot1 noot2*, ectopic roots also can be formed from aborted nodule primordia inoculated with inf$^-$ mutant rhizobia. This result shows that *MtNOOT* genes control the activity of the NVM in an infection-independent manner. Homeotic mutants often represent a step back in evolution and highlight the evolutionary pathway giving rise to a new organ. The nodule-to-root reversion phenotype confirms that the nodule vasculature is ontologically related to roots.

Transcript accumulation analysis of RAM markers suggests that the auxin-related root-derived developmental program recruited for the functioning of NVB initials is up-regulated in *Mtnoot1* and *Mtnoot1 noot2* nodules. In R-108 nodules, the expression of *MtPLT2* is associated mostly with the NVM (Roux et al., 2014; Franssen et al., 2015). In R-108 nodules, we show that *MtPLT2* expression is controlled strictly from nodule primordia establishment to the subsequent stages of nodule development, while in *Mtnoot1* and *Mtnoot1 noot2*, *MtPLT2* expression is strongly up-regulated. These observations are in agreement with the hypothesis that the auxin-related root-derived developmental program recruited to initiate NVB formation is reactivated in the mutants.

In Arabidopsis, *AtBOP* genes participate in the definition of boundary domains within and between organs to ensure their correct development (Ha et al., 2003, 2004; Hepworth et al., 2005; Norberg et al., 2005; Jun et al., 2010; for review, see Žádníková and Simon, 2014; Hepworth and Pautot, 2015; Wang et al., 2016). In *M. truncatula* indeterminate nodules, *Mt*NOOTs may play a similar role in the definition and regulation of the boundary zone between NVM and NCM. In addition, *Mt*NOOTs may indirectly coordinate the expression of RAM-related genes in adjacent domains (i.e. NCM and NVM) to allow harmonious nodule development and to maintain nodule identity. Additional experiments using RAM marker gene expression patterns in *Mtnoot* mutants should help to better understand the molecular mechanisms underlying the nodule-to-root homeosis and, thus, nodule identity regulation.

In this study, we also demonstrate that the loss of nodule identity triggers the accumulation of salicylic acid in *Mtnoot1* mutant nodules, the up-regulation of defense-related marker genes, and the degeneration of nodule infected cells leading to a fix$^-$ phenotype. These observations suggest that a major modification of the immune status occurs in *Mtnoot1* and *Mtnoot1 noot2* converted nodules.

The loss of nodule identity also is associated with a decrease in symbiotic gene expression. In *Mtnoot1* and *Mtnoot1 noot2*, the expression of early symbiotic genes (*MtCRE* and *MtNIN*) was less affected than the expression of late symbiotic genes (*MtNCR001*, *MtLEGH1*, *MtDNF2*, and *MtSymCRK*) that were impacted drastically. This suggested that *Mt*NOOT loss of function has a reduced impact during the early steps of nodule primordium development and a high impact when the nodule starts to become functional.

Together, the modification of the immune status and the decrease in symbiotic marker gene expression show that, during nodule development, symbiotic identity acquisition is probably a key point for hosting the bacterial symbiont (Gourion et al., 2015). The particular nodule immune status allowing chronic bacterial infection and a massive bacterial accommodation might be associated with the acquisition of nodule identity.

Role of the Class II *MtKNOX* Genes in Nodule Identity

In *M. truncatula*, class II KNOX TFs regulate nodule development (Azarakhsh et al., 2015; Di Giacomo et al., 2016). The class II *MtKNOX3*, *MtKNOX5*, and *MtKNOX9* genes are induced during symbiosis, appearing to be functionally redundant and contributing to the regulation of proper nodule size, boundary, and shape (Di Giacomo et al., 2016). The MtKNOX3 gene is described as required for the expression of *MtADENYLATE ISOPENTHENYL TRANSFERASE3* (*MtIPT3*) and *MtLONELY GUY2* (*MtLOG2*), two key genes encoding enzymes involved in cytokinin signaling during nodule development (Azarakhsh et al., 2015).

In *Mtnoot1* and *Mtnoot1 noot2*, as for RAM gene expression changes, the class II MtKNOX expression changes suggest hormonal perturbations. Indeed, as in *MtKNOX3*:RNA interference mutant lines (Azarakhsh et al., 2015), the drastic down-regulation of *MtKNOX3* observed in *Mtnoot1* and *Mtnoot1 noot2* nodules probably reduces the accumulation of *MtIPT3* and *MtLOG2* transcripts. In consequence, a reduced level of cytokinin and/or of its active forms could alter nodule development and identity.

In *Mtnoot1* and *Mtnoot1 noot2* nodules, the up-regulation of RAM gene markers and the down-regulation of *MtKNOX3* expression might reflect an auxin/cytokinin imbalance. Such hormonal perturbations

might be involved in the nodule-to-root identity conversion.

In addition to the reduced expression of class II *MtKNOX3* and *MtKNOX9*, a drastic rearrangement of the *ProKNOX9:GUS* expression pattern was observed in *Mtnoot1* and *Mtnoot1 noot2* nodules. In nodules that have lost their identity, the NM-associated *ProKNOX9:GUS* expression pattern was lost and the gene expression of *MtKNOX9* was reactivated in the NVBs as in a wild-type root context (Di Giacomo et al., 2016). The *ProKNOX9:GUS* expression pattern shift correlates with nodule-to-root homeosis but also supports the role of *MtKNOX9* in nodule identity, as proposed previously for class II KNOX TFs (Di Giacomo et al., 2016). A molecular mechanism involving class II MtKNOX TF may have been recruited from the preexisting root developmental program to build the nodule and define its identity in an *Mt*NOOT1-dependent manner.

Our study identifies and characterizes *Mt*NOOT2, the paralog of *Mt*NOOT1 in *M. truncatula*, as a molecular actor involved in the regulation of indeterminate nodule identity and provides insights into the molecular basis underlying nodule identity. How legumes acquired their nodule organogenesis program during evolution is not yet known, but it appears that, to form nodules, legumes have recycled preexisting root developmental programs and modulated their domains of expression within the nodule. The *Mtnoot* mutants described in this work represent valuable genetic tools that will undoubtedly help to better understand the molecular mechanisms underlying the regulation of nodule identity in future studies.

MATERIALS AND METHODS

Plant Material and Growth Conditions

Wild-type *Medicago truncatula* ecotype R-108 (Hoffmann et al., 1997) and its corresponding mutants *Mtnoot1* (Tnk507 and NF2717; Couzigou et al., 2012), *Mtnoot2* (NF5464 and NF5722; this study), *Mtnoot1 noot2* (NF2717 [back-crossed once] crossed with NF5464 [back-crossed once]; this study), R-108 *ProNOOT1:GUS* (Couzigou et al., 2012), R-108 *ProNOOT2:GUS* (this study), *Mtnoot1 ProNOOT2:GUS* (R-108 *ProNOOT2:GUS* crossed with *Mtnoot1* Tnk507; this study), and *Mtnoot2 ProNOOT1:GUS* (R-108 *ProNOOT1:GUS* crossed with *Mtnoot2* NF5464; this study) were cultivated on a perlite and sand mix (3:1, v/v) or on buffered nodulation medium in vitro plates (Ehrhardt et al., 1992) solidified with Kalys agar (7 g L^{-1}) and supplemented with 0.5 µM 2-aminoethoxyvinylglycine. Plants were grown in a controlled environmental chamber with a 16/8-h light/dark cycle, 24°C/24°C day/night temperature, relative humidity of 60%, and 200 µE light intensity. Plants cultivated in the sand-perlite mixture were watered with 1 g L^{-1} N-free nutritive solution (Plant-Prod NPK 0-15-40).

Bacterial Strains and Growth Conditions

M. truncatula nodulation assays were performed as described by Berrabah et al. (2015) with *Sinorhizobium medicae* WSM419 (Howieson and Ewing, 1986), *S. medicae* WSM419 eGFP, *Sinorhizobium meliloti* Rm41 (Kondorosi et al., 1984), Rm41 *kps*$^-$ (PP711; Becquart-de Kozak et al., 1997), Rm41 *exo*$^-$ (AK631; Putnoky et al., 1988), or Rm41 *exo*$^-$ *kps*$^-$ (PP666; Putnoky et al., 1990). Rhizobia were cultivated on yeast extract beef medium (Krall et al., 2002) for 2 d at 30°C, and plant roots were inoculated with suspensions at an OD_{600} of 0.1.

Yeast Strain and Growth Conditions

Saccharomyces cerevisiae strain AH109 (James et al., 1996; A. Holtz, unpublished data) was used for yeast two-hybrid approaches. AH109 yeast were grown on solid yeast extract peptone dextrose (YPD) agar (Y1500; Sigma-Aldrich) for 2 d at 30°C or in liquid YPD broth (Y1375; Sigma-Aldrich) at 30°C, under 180 rpm agitation. Cotransformed AH109 yeast strains were grown for 2 d at 30°C on minimal SD–L–W agar (Clontech; 630412 and 630417) or for 16 to 18 h at 30°C in 5 mL of minimal SD–L–W broth (Clontech; ST0047) under 230 to 270 rpm agitation until $OD_{600} > 1.5$.

Phylogenetic Tree Construction

Full-length NBCL protein sequences of different species from Fabaceae, Brassicaceae, Solanaceae, Poaceae, and Zosteraceae families were obtained from the National Center for Biotechnology Information BLAST search portal (https://blast.ncbi.nlm.nih.gov/). Sequences were aligned using MUSCLE (Edgar, 2004, and the phylogenetic tree was built using the maximum likelihood-based method and the Jones-Taylor-Thornton substitution model with the MEGA6 program (Tamura et al., 2013). The tree was rooted with NBCL sequences from the basal monocot *Zostera marina* (Olsen et al., 2016). The tree was drawn according to the evolutionary distances, based on the proportion of amino acid differences between sequences, and was established using pairwise distance analysis using the MEGA6 program (Tamura et al., 2013). The maximum-likelihood tree was evaluated using 1,000 bootstrap replicates. NBCL1 and NBCL2 protein sequence identity percentages were determined using the MATrix Global Alignment Tool software version 2.01 (Campanella et al., 2003; http://www.angelfire.com/nj2/arabidopsis/MatGAT.html). Information concerning NBCL protein sequences used in the phylogenetic analysis are provided in Supplemental Table S1.

M. truncatula DNA Extraction and *Tnt1* Insertional Mutant Genotyping

M. truncatula DNA was extracted from young leaves using a phenol-chloroform procedure. DNA was precipitated using cold sodium acetate (3 M):isopropanol (0.1:1) and washed using 70% (v/v) ethanol. DNA samples were dried and resuspended in sterile water. Finally, an RNase treatment was performed (Roche). The *M. truncatula Mtnoot1* (Tnk507 and NF2717) and *Mtnoot2* (NF5464 and 5722) *Tnt1* insertional lines were genotyped by semiquantitative PCR using DreamTaq DNA Polymerase (EP0701; Thermo Fisher Scientific). Information concerning the primers used for *Tnt1* insertional mutant genotyping are provided in Supplemental Table S2.

RT-qPCR Gene Expression Analysis

Total RNA extractions were performed from frozen tissues using TRIzol reagent (Ambion). RNA samples were treated with the TURBO DNA-free Kit (Ambion) according to the manufacturer's recommendations. Full-length cDNA was synthesized using the SuperScript II Reverse Transcriptase kit (Invitrogen) in the presence of Ribolock RNase Inhibitor (Thermo Scientific). RT-qPCR was performed using the LightCycler FastStart DNA Master SYBR Green I kit and a Light Cycler 480 II according to the manufacturer's instructions (Roche). Cycling conditions were as follows: one preincubation cycle (95°C for 10 min), 40 amplification cycles (denaturation, 95°C for 10 s; hybridization, 60°C for 15 s; and elongation, 72°C for 15 s), one melting curve cycle (denaturation, 95°C for 15 s; hybridization, 55°C for 1 min; and denaturation, 95°C), and one cooling cycle (40°C for 30 s). Cycle threshold and primer specificities were determined with the LightCycler 480 software release 1.5.0 SP4. Primer efficiencies were calculated with LinReg PCR: Analysis of Real-Time PCR Data, version 11.1. *MtACT11* and *MtRNA RECOGNITION MOTIF* reference genes were used for gene expression normalization. Information concerning the primers used for RT-qPCR gene expression analyses is provided in Supplemental Table S3.

Promoter:*GUS* Reporter Fusion Construction

For *ProMtNOOT2:GUS* construction, 2,534 bp of the *MtNOOT2* promoter region including the 5′ untranslated region plus the region encoding the first 15 amino acids of the MtNOOT2 protein was amplified using Phusion

polymerase (Thermo Fisher Scientific), the reverse primer (5′-GGATCCAGGTAGTCAAGGGAGAGAGATCTT-3′), and the forward primer (5′-CGCCCCATTGCCATGCCTATATATC-3′). The amplified fragment was cloned into pGEM-T Easy vector (Promega) and sequenced. The *MtNOOT2* promoter region was cloned into the pPR97 vector (Szabados et al., 1995) using *Bam*HI-*Eco*RI restriction enzymes. For *ProKNOX9:GUS* construction, sequence information for the promoter and terminator regions of Medtr4g116545 was obtained from the *M. truncatula* Mt4.0v1 genome (https://phytozome.jgi.doe.gov; Goodstein et al., 2012). Sequences were synthesized by GeneArt (Life Technology) as level 0 modules for Golden Gate cloning (Weber et al., 2011; https://www.ensa.ac.uk/). The *MtKNOX9* promoter (2,777 bp), the GUS coding sequence (2,016 bp), and the *MtKNOX9* terminator (1,369 bp) were assembled to a level 1 module and combined with the *ProAtUBIQUITIN:DsRed* (*Discosoma* sp. red fluorescent protein) level 1 module into the binary level 2 vector EC15025 (https://www.ensa.ac.uk/).

Agrobacterium tumefaciens-Mediated Plant Transformation

M. truncatula transgenic plants expressing the *ProNOOT2:GUS* fusion were generated as described by Cosson et al. (2015). Eight independent transgenic plants were analyzed, and seven showed a similar NCM-associated *ProNOOT2:GUS* expression pattern.

Agrobacterium rhizogenes-Mediated Root Transformation

For *ProNOOT2:GUS*, *M. truncatula* Jemalong J5 hairy root transformation was performed as described by Boisson-Dernier et al. (2001) using *A. rhizogenes* A4TC24. The transgenic roots were grown for 2 weeks on Fahraeus medium (Fahraeus, 1957) containing 1.5% (w/v) Kalys agar (HP696-5) and selected using kanamycin (25 mg L^{-1}). Transgenic roots were transferred on buffered nodulation medium plates containing 0.5 µM 2-aminoethoxyvinylglycine for 3 d before inoculation with WSM419 (15 mL per plate). Nodules were collected every 2 d from 4 to 15 dpi for subsequent histochemical GUS analyses. For *ProKNOX9:GUS*, R-108, *Mtnoot1*, and *Mtnoot1 noot2* hairy root transformation was performed as described by Boisson-Dernier et al. (2001) using *A. rhizogenes* AR1193. The transgenic roots were selected by fluorescence microscopy using the *ProAtUBIQUITIN:DsRed* reporter. Transgenic roots were transferred to a Terragreen:Sharp Sand Mix (1:1; Oil-DriCompany) and inoculated with *S. meliloti* Sm2011. Nodules were collected at 28 dpi for subsequent histochemical GUS analysis.

Light Microscopy and Sample Preparation

Histochemical GUS staining was performed as described previously by Pichon et al. (1992). Samples were prefixed in 90% (v/v) cold acetone for 1 h at −20°C. Samples were vacuum infiltrated for 30 min (~500 mm Hg) in X-gluc staining buffer (50 mM phosphate buffer, pH 7.2, 1 mM potassium ferricyanide, 1 mM potassium ferrocyanide, 0.1% (w/v) SDS, 1 mM EDTA, and 1.25 mM 5-bromo-4-chloro-3-indolyl-beta-D-GlcA containing cyclohexylammonium salt) and incubated at 37°C, overnight, under darkness. Samples were fixed in 100 mM phosphate buffer, pH 7.2, 1% (v/v) glutaraldehyde, and 4% (v/v) formaldehyde for 2 h under vacuum (~500 mm Hg).

Methylene Blue staining of vascular tissues was performed as described by Truchet et al. (1989). Whole root systems were vacuum infiltrated for 15 min (~500 mm Hg) in 6% (v/v) sodium hypochlorite and left for 15 min under atmospheric pressure. Samples were washed three times with sterile water, incubated for 1 h in 0.04% (w/v) $KMNO_4$, and washed with sterile water. Samples were stained with 0.01% (w/v) Methylene Blue for 20 min, cleared with 6% (v/v) sodium hypochlorite for approximately 2 min, and finally washed with sterile water.

For semithin sections (60 µm thickness), samples were embedded in 6% (w/v) agarose and sliced with a vibratome (VT1200S; Leica) in 50 mM Tris-HCl, pH 7.5. Images were obtained using a Macroscope AZ100 (Nikon) and the NIS element software (Nikon). Image stacks were performed using ImageJ.

Technovit sectioning was performed as described by Van de Velde et al. (2006). Samples were fixed in 0.05 M sodium cacodylate buffer, pH 7, 1% (v/v) glutaraldehyde, and 4% (v/v) formaldehyde by 15 min of infiltration under vacuum (~500 mm Hg) and incubated overnight at 4°C. Once dehydrated by successive ethanol baths, samples underwent three successive Technovit stock solution (3:1 [v/v], 1:1 [v/v], and 1:3 [v/v]) baths and three 1-h 100% Technovit stock solution baths at 4°C under agitation. Samples were included in Technovit resin using Teflon Histoform S embedding molds (Heraeus Kulzer). Technovit sectioning was carried out using an RM 2155 microtome (Leica) and tungsten disposable blade (TC-65; Leica). For GUS stained samples counterstained with 0.05% (w/v) Ruthenium Red and for samples stained with 0.02% (w/v) Toluidine Blue, 7-and 5-µm-thick sections were made, respectively. .

RNA in Situ Hybridization

In situ hybridizations were performed as described by Bustos-Sanmamed et al. (2013) on 28-dpi nodules of *M. truncatula* R-108 inoculated with WSM419 and using an Intavis InsituPro automat. Primers used for the synthesis of the specific RNA probe targeting either *MtNOOT1* or *MtNOOT2* are provided in Supplemental Table S4.

Yeast Two-Hybrid Vector Construction

PCR amplification of *MtNOOT1* (1,452 bp) and *MtNOOT2* (1,479 bp) coding sequences was carried out using R-108 nodule cDNA and High Fidelity Taq DNA polymerase (EUROBIO GAETHF004D). Information concerning primers used for cDNA amplification is given in Supplemental Table S5. PCR products were sequenced (www.eurofinsgenomics.eu). For cloning, 3′ adenine was added to the PCR products using Dream Taq DNA polymerase (Thermo Fisher Scientific), then purified with the GeneJET PCR Purification Kit (Thermo Fisher Scientific), cloned into the pGEM-T Easy vector using pGEM-T Easy Vector System I (Promega), and introduced into One Shot TOP10 chemically competent *Escherichia coli* cells (Thermo Fisher Scientific). pGEM-T Easy vectors containing *MtNOOT* cDNA were sequenced (www.eurofinsgenomics.eu) using T7 and SP6 universal oligonucleotides (Supplemental Table S5). Subcloning of *MtNOOT1* and *MtNOOT2* full-length cDNA was carried out by restriction enzyme digestion of the pGEM-T Easy constructs using *Nde*I/*Bam*HI and *Nde*I/*Xma*I (New England Biolabs) combinations, respectively. Inserts from pGEM-T Easy vectors and linearized pGADT7 AD and pGBKT7 destination vectors (Clontech Laboratories) were purified with NucleoSpin Gel and PCR Clean-up (Macherey Nagel). Each cDNA was subcloned using T4 DNA ligase (Thermo Fisher Scientific) into both pGADT7 AD and pGBKT7 destination vectors and introduced into One Shot TOP10 cells. pGADT7 AD:*MtNOOT1*, pGADT7 AD:*MtNOOT2*, pGBKT7:*MtNOOT1*, and pGBKT7:*MtNOOT2* constructs were sequenced (www.eurofinsgenomics.eu) and their orientations in the respective vectors were checked. Information concerning oligonucleotides used for sequencing in pGADT7 AD and pGBKT7 is provided in Supplemental Table S5.

Yeast Cotransformation

Yeast transformations were performed using the lithium acetate (LiAc) method (Gietz and Schiestl, 1995) with some modifications. Fresh AH109 liquid culture was performed during 24 h until an OD_{600} of 2.6. The culture was diluted in fresh prewarmed liquid YPD to OD_{600} = 0.2 to 0.25 and grown for 3 to 6 h to obtain $0.4 < OD_{600} < 0.6$. Fifty milliliters of the culture was centrifuged 5 min at 1.1*g*, resuspended in 25 mL of sterile water, centrifuged 5 min at 1.1*g*, resuspended in 1 mL of freshly prepared 0.1 M LiAc, pH 7.5 (L-4158; Sigma-Aldrich), transferred to a 2-mL tube and full speed centrifuged for 15 s, and finally resuspended in 400 µL of 0.1 M LiAc, pH 7.5. Cotransformations were performed in 2-mL tubes in the presence of 250 ng of each construct, 50 µL of yeast cell suspension, 240 µL of sterile 50% (w/v) polyethylene glycol (p-3640; Sigma-Aldrich), 36 µL of sterile 1 M LiAc, pH 7.5, 64 µL of sterile water, and 10 µL of 10 mg mL^{-1} denaturated single-stranded DNA from salmon testes (D7656; Sigma-Aldrich). Mixtures were vortexed for 30 s, incubated for 30 min at 30°C under 200 rpm agitation, and the tubes were inverted every 10 min. Yeast cells were incubated at 42°C during 30 min, centrifuged at 4.2*g* for 15 s, resuspended in 200 µL of sterile water, and grown for 4 to 7 d on minimal SD–L–W agar to select cotransformed yeast colonies.

Yeast Two-Hybrid Growth Assay

Protein-protein interactions were performed by assessing the growth fitness of cotransformed yeast. Cotransformed yeast were grown overnight and under agitation in 1 mL of minimal SD–L–W broth on 96-well plates (Greiner bio-one; Masterblock; 780271) and sealed with adhesive gas-permeable seals (Thermo Scientific; AB-0718). The overnight cultures were diluted

100-fold in sterile water, and 5 µL of each dilution was dropped on minimal SD–L–W–H–A (630412 and 630428; Clontech) supplemented with 1 mM 3-amino-1,2,4-triazole (Sigma-Aldrich; A8056).

Acetylene Reduction Assay

Acetylene reduction assays were performed on individual plant root systems inoculated with WSM419 at 35 dpi with a protocol modified from Koch and Evans (1966). Basically, the nodulated root system of a single plant was placed in a 21-mL glass vial sealed with a rubber septum in the presence of 200 µL of water. Acetylene gas (500 µL) was injected into each vial, and a 2-h incubation was performed. For each sample, 1 mL of gas was injected. Ethylene production was measured by gas chromatography using a gas chromatograph (7820A; Agilent Technologies) equipped with a GS-Alumina column (50 m × 0.53 mm). Hydrogen was used as the carrier gas. Column temperature and gas flow were 120°C and 7.5 mL min^{-1}, respectively.

Salicylic Acid Quantification

For each root and nodule sample, 3 and 4 mg of dry powder were extracted with 0.8 mL of acetone:water:acetic acid (80:19:1, v/v/v), respectively. Salicylic acid, jasmonic acid, indole-3-acetic acid, and cytokinins labeled with stable isotopes were used as internal standards and prepared as described by Le Roux et al. (2014). Two nanograms of each hormone standard (or 0.5 ng of cytokinins) was added to the samples. The extract was shaken vigorously for 1 min, sonicated for 1 min at 25 Hz, shaken for 10 min at 10°C in a Thermomixer (Eppendorf), and then centrifuged (8,000*g*, 10°C, 10 min). The supernatants were collected, and the pellets were reextracted twice with 0.4 mL of the same extraction solution, then shaken vigorously (1 min) and sonicated (1 min; 25 Hz). After the centrifugations, the three supernatants were pooled and dried (final volume of 1.6 mL). Each dry extract was dissolved in 100 µL of acetonitrile:water (50:50, v/v), filtered, and analyzed using a Waters Acquity ultra-performance liquid chromatograph coupled to a Waters Xevo triple quadrupole mass spectrometer. The compounds were separated using a reverse-phase column (Uptisphere C18 UP3HDO; 100 × 2.1 mm × 3 µm particle size; Interchim) at a flow rate of 0.4 mL min^{-1} and a binary gradient of 0.1% (v/v) acetic acid in water (A) and acetonitrile with 0.1% (v/v) acetic acid (B); the column temperature was 40°C. For abscisic acid, salicylic acid, jasmonic acid, and indole-3-acetic acid, we used the following binary gradient (time, % A): 0 min, 98%; 3 min, 70%; 7.5 min, 50%; 8.5 min, 5%; 9.6 min, 0%; 13.2 min, 98%; and 15.7 min, 98%. For cytokinins, the following binary gradient was used (time, % A): 0 min, 95%; 13 min, 40%; 16 min, 0%; and 16.5 min, 95%. Mass spectrometry was conducted in electrospray and multiple reaction monitoring scanning mode, in positive ion mode for the indole-3-acetic acid, and in negative ion mode for the other hormones. Relevant instrumental parameters were set as follows: capillary, 1.5 kV (negative mode); source block and desolvation gas temperatures, 130°C and 500°C, respectively. Nitrogen was used to assist the cone and desolvation (150 and 800 L h^{-1}, respectively), and argon was used as the collision gas at a flow rate of 0.18 mL min^{-1}.

Accession Numbers

Accession numbers are listed in Supplemental Tables S1 and S3.

Supplemental Data

The following supplemental materials are available.

Supplemental Figure S1. Alignment of legume NBCL2 proteins.

Supplemental Figure S2. *ProNOOT1:GUS* and *ProNOOT2:GUS* expression patterns during R-108 nodulation.

Supplemental Figure S3. *MtNOOT1* in situ RNA hybridization in R-108 nodules.

Supplemental Figure S4. MtNOOT1 and MtNOOT2 form homodimers and heterodimers in yeast.

Supplemental Figure S5. *Mtnoot1 noot2* inoculation with *exo*$^-$, *kps*$^-$, and *exo*$^-$ *kps*$^-$ rhizobial mutants.

Supplemental Figure S6. In toto *ProNOOT2:GUS* expression pattern in *Mtnoot1*.

Supplemental Figure S7. *MtPLT1* to *MtPLT4* expression during R-108 nodulation and in *Mtnoot* mutant nodules.

Supplemental Figure S8. Salicylic acid accumulates in *Mtnoot1* nodules.

Supplemental Figure S9. Class II *MtKNOX3*, *MtKNOX5*, and *MtKNOX9* expression in *Mtnoot* mutants.

Supplemental Table S1. List of *NBCL* genes and proteins used in this study.

Supplemental Table S2. Primers used for *Tnt1* insertional mutant genotyping.

Supplemental Table S3. Primers used for RT-qPCR gene expression analysis.

Supplemental Table S4. Primers used for RNA in situ hybridization.

Supplemental Table S5. Primers used for yeast two-hybrid approaches.

Supplemental References.

ACKNOWLEDGMENTS

We thank the Observatoire du Végétal-Chimie Métabolisme Plateform for salicylic acid quantifications; Dr. Gabriella Endre from the Biological Research Centre of Szeged for providing *S. medicae* WSM419 eGFP; Carole Laffont from the IPS2 for providing fixed R-108 nodules for in situ RNA hybridizations; and Dr. Michael Hodges from the IPS2 for article revision and English language editing.

Received May 21, 2018; accepted July 6, 2018; published July 19, 2018.

LITERATURE CITED

Aida M, Beis D, Heidstra R, Willemsen V, Blilou I, Galinha C, Nussaume L, Noh YS, Amasino R, Scheres B (2004) The PLETHORA genes mediate patterning of the Arabidopsis root stem cell niche. Cell **119**: 109–120

Alves-Carvalho S, Aubert G, Carrère S, Cruaud C, Brochot AL, Jacquin F, Klein A, Martin C, Boucherot K, Kreplak J, (2015) Full-length de novo assembly of RNA-seq data in pea (*Pisum sativum* L.) provides a gene expression atlas and gives insights into root nodulation in this species. Plant J **84**: 1–19

Azarakhsh M, Kirienko AN, Zhukov VA, Lebedeva MA, Dolgikh EA, Lutova LA (2015) KNOTTED1-LIKE HOMEOBOX **3**: a new regulator of symbiotic nodule. J Exp Bot **66**: 7181–7195

Becquart-de Kozak I, Reuhs BL, Buffard D, Breda C, Kim JS, Esnault R, Kondorosi A (1997) Role of the K-antigen subgroup of capsular polysaccharides in the early recognition process between *Rhizobium meliloti* and alfalfa leaves. Mol Plant Microbe Interact **10**: 114–123

Benedito VA, Torres-Jerez I, Murray JD, Andriankaja A, Allen S, Kakar K, Wandrey M, Verdier J, Zuber H, Ott T, (2008) A gene expression atlas of the model legume *Medicago truncatula*. Plant J **55**: 504–513

Berrabah F, Bourcy M, Cayrel A, Eschstruth A, Mondy S, Ratet P, Gourion B (2014a) Growth conditions determine the DNF2 requirement for symbiosis. PLoS ONE **9**: e91866

Berrabah F, Bourcy M, Eschstruth A, Cayrel A, Guefrachi I, Mergaert P, Wen J, Jean V, Mysore KS, Gourion B, (2014b) A nonRD receptor-like kinase prevents nodule early senescence and defense-like reactions during symbiosis. New Phytol **203**: 1305–1314

Berrabah F, Ratet P, Gourion B (2015) Multiple steps control immunity during the intracellular accommodation of rhizobia. J Exp Bot **66**: 1977–1985

Berrabah F, Balliau T, Aït-Salem EH, George J, Zivy M, Ratet P, Gourion B (2018) Control of the ethylene signaling pathway prevents plant defenses during intracellular accommodation of the rhizobia. New Phytol **219**: 310–323

Blixt S (1967) Linkage studies in Pisum. VII. The manifestation of the genes cri, and coch, and the double-recessive in Pisum. Agric Hortic Genet **25**: 131–144

Boisson-Dernier A, Chabaud M, Garcia F, Bécard G, Rosenberg C, Barker DG (2001) *Agrobacterium rhizogenes*-transformed roots of *Medicago truncatula* for the study of nitrogen-fixing and endomycorrhizal symbiotic associations. Mol Plant Microbe Interact **14**: 695–700

Bonfante P, Genre A (2010) Mechanisms underlying beneficial plant-fungus interactions in mycorrhizal symbiosis. Nat Commun **1**: 48

Bourcy M, Berrabah F, Ratet P, Gourion B (2013a) Failure of self-control. Plant Signal Behav **8**: e23915

Bourcy M, Brocard L, Pislariu CI, Cosson V, Mergaert P, Tadege M, Mysore KS, Udvardi MK, Gourion B, Ratet P (2013b) Medicago truncatula DNF2 is a PI-PLC-XD-containing protein required for bacteroid persistence and prevention of nodule early senescence and defense-like reactions. New Phytol **197**: 1250–1261

Bustos-Sanmamed P, Laffont C, Frugier F, Lelandais-Brière C, Crespi M (2013) Analyzing small and long RNAs in plant development using non-radioactive in situ hybridization. Methods Mol Biol **959**: 303–316

Campanella JJ, Bitincka L, Smalley J (2003) MatGAT: an application that generates similarity/identity matrices using protein or DNA sequences. BMC Bioinformatics **4**: 29

Combier JP, Frugier F, de Billy F, Boualem A, El-Yahyaoui F, Moreau S, Vernié T, Ott T, Gamas P, Crespi M, (2006) MtHAP2-1 is a key transcriptional regulator of symbiotic nodule development regulated by microRNA169 in Medicago truncatula. Genes Dev **20**: 3084–3088

Combier JP, de Billy F, Gamas P, Niebel A, Rivas S (2008) Trans-regulation of the expression of the transcription factor MtHAP2-1 by a uORF controls root nodule development. Genes Dev **22**: 1549–1559

Cosson V, Eschstruth A, Ratet P (2015) Medicago truncatula transformation using leaf explants. *In* **K Wang**, ed, Agrobacterium Protocols, Ed 3. Humana Press, Totowa, NJ, pp 43–56

Couzigou JM, Ratet P (2015) NOOT-dependent control of noduleidentity: nodule homeosis and meristem perturbation. In Biological Nitrogen Fixation, Vol.1 (**de Bruijn, F.J. ed.**), Hoboken, NJ: Wiley. pp. 487–497. 10.1002/9781119053095.ch49

Couzigou JM, Zhukov V, Mondy S, Abu el Heba G, Cosson V, Ellis TH, Ambrose M, Wen J, Tadege M, Tikhonovich I, (2012) *NODULE ROOT* and *COCHLEATA* maintain nodule development and are legume orthologs of *Arabidopsis BLADE-ON-PETIOLE* genes. Plant Cell **24**: 4498–4510

Couzigou JM, Mondy S, Sahl L, Gourion B, Ratet P (2013) To be or noot to be? Evolutionary tinkering for symbiotic organ identity. Plant Signal Behav **8**: e24969

Couzigou JM, Magne K, Mondy S, Cosson V, Clements J, Ratet P (2016) The legume NOOT-BOP-COCH-LIKE genes are conserved regulators of abscission, a major agronomical trait in cultivated crops. New Phytol **209**: 228–240 10.1111/nph.1363426390061

Cui H, Levesque MP, Vernoux T, Jung JW, Paquette AJ, Gallagher KL, Wang JY, Blilou I, Scheres B, Benfey PN (2007) An evolutionarily conserved mechanism delimiting SHR movement defines a single layer of endodermis in plants. Science **316**: 421–425

Di Giacomo E, Laffont C, Sciarra F, Iannelli MA, Frugier F, Frugis G (2016) KNAT3/4/5-like class 2 KNOX transcription factors are involved in *Medicago truncatula* symbiotic nodule organ development. New Phytol **213**: 822–837

Edgar RC (2004) MUSCLE: multiple sequence alignment with high accuracy and high throughput. Nucleic Acids Res **32**: 1792–1797

Ehrhardt DW, Atkinson EM, Long SR (1992) Depolarization of alfalfa root hair membrane potential by *Rhizobium meliloti* Nod factors. Science **256**: 998–1000

Fahraeus G (1957) The infection of clover root hairs by nodule bacteria studied by a simple glass slide technique. J Gen Microbiol **16**: 374–381

Ferguson BJ, Reid JB (2005) *Cochleata*: getting to the root of legume nodules. Plant Cell Physiol **46**: 1583–1589

Frankowski K, Wilmowicz E, Kućko A, Zienkiewicz A, Zienkiewicz K, Kopcewicz J (2015) Molecular cloning of the BLADE-ON-PETIOLE gene and expression analyses during nodule development in Lupinus luteus. J Plant Physiol **179**: 35–39

Franssen HJ, Xiao TT, Kulikova O, Wan X, Bisseling T, Scheres B, Heidstra R (2015) Root developmental programs shape the *Medicago truncatula* nodule meristem. Development **142**: 2941–2950

Furumizu C, Alvarez JP, Sakakibara K, Bowman JL (2015) Antagonistic roles for KNOX1 and KNOX2 genes in patterning the land plant body plan following an ancient gene duplication. PLoS Genet **11**: e1004980

Gietz RD, Schiestl RH (1995) Transforming yeast with DNA. Methods Mol Cell Biol **5**: 255–269

Gonzalez-Rizzo S, Crespi M, Frugier F (2006) The *Medicago truncatula* CRE1 cytokinin receptor regulates lateral root development and early symbiotic interaction with *Sinorhizobium meliloti*. Plant Cell **18**: 2680–2693

Goodstein DM, Shu S, Howson R, Neupane R, Hayes RD, Fazo J, Mitros T, Dirks W, Hellsten U, Putnam N, (2012) Phytozome: a comparative platform for green plant genomics. Nucleic Acids Res **40**: D1178–D1186

Gourion B, Berrabah F, Ratet P, Stacey G (2015) Rhizobium-legume symbioses: the crucial role of plant immunity. Trends Plant Sci **20**: 186–194

Gourlay CW, Hofer JMI, Ellis THN (2000) Pea compound leaf architecture is regulated by interactions among the genes UNIFOLIATA, COCHLEATA, AFILA and TENDRIL-LESS. Plant Cell **12**: 1279–1294

Guinel FC (2009) Getting around the legume nodule. I. The structure of the peripheral zone in four nodule types. Botany **87**: 1117–1138

Ha CM, Kim GT, Kim BC, Jun JH, Soh MS, Ueno Y, Machida Y, Tsukaya H, Nam HG (2003) The *BLADE-ON-PETIOLE 1* gene controls leaf pattern formation through the modulation of meristematic activity in *Arabidopsis*. Development **130**: 161–172

Ha CM, Jun JH, Nam HG, Fletcher JC (2004) BLADE-ON-PETIOLE1 encodes a BTB/POZ domain protein required for leaf morphogenesis in *Arabidopsis thaliana*. Plant Cell Physiol **45**: 1361–1370

Hake S, Smith HMS, Holtan H, Magnani E, Mele G, Ramirez J (2004) The role of KNOX genes in plant development. Annu Rev Cell Dev Biol **20**: 125–151

Hay A, Tsiantis M (2010) KNOX genes: versatile regulators of plant development and diversity. Development **137**: 3153–3165

He J, Benedito VA, Wang M, Murray JD, Zhao PX, Tang Y, Udvardi MK (2009) The *Medicago truncatula* gene expression atlas web server. BMC Bioinformatics **10**: 441

Hepworth SR, Pautot VA (2015) Beyond the divide: boundaries for patterning and stem cell regulation in plants. Front Plant Sci **6**: 1052

Hepworth SR, Zhang Y, Mckim S, Li X, Haughn GW (2005) BLADE-ON-PETIOLE: dependent signaling controls leaf and floral patterning in Arabidopsis. Plant Cell **17**: 1434–1448

Herrbach V, Chirinos X, Rengel D, Agbevenou K, Vincent R, Pateyron S, Huguet S, Balzergue S, Pasha A, Provart N, (2017) Nod factors potentiate auxin signaling for transcriptional regulation and lateral root formation in Medicago truncatula. J Exp Bot **68**: 569–583

Hoffmann B, Trinh TH, Leung J, Kondorosi A, Kondorosi E (1997) A new *Medicago truncatula* line with superior in vitro regeneration, transformation, and symbiotic properties isolated through cell culture selection. Mol Plant Microbe Interact **10**: 307–315

Horvath B, Heidstra R, Lados M, Moerman M, Spaink HP, Promé J, van Kammen A, Bisseling T (1993) Lipo-oligosaccharides of Rhizobium induce infection-related early nodulin gene expression in pea root hairs. Plant J **4**: 727–733

Howieson JG, Ewing MA (1986) Acid tolerance in the *Rhizobium meliloti-Medicago symbiosis*. Aust J Agric Res **37**: 55–64

Humphreys CP, Franks PJ, Rees M, Bidartondo MI, Leake JR, Beerling DJ (2010) Mutualistic mycorrhiza-like symbiosis in the most ancient group of land plants. Nat Commun **1**: 103

James P, Halladay J, Craig EA (1996) Genomic libraries and a host strain designed for highly efficient two-hybrid selection in yeast. Genetics **144**: 1425–1436

Jones KM, Kobayashi H, Davies BW, Taga ME, Walker GC (2007) How rhizobial symbionts invade plants: the Sinorhizobium-Medicago model. Nat Rev Microbiol **5**: –633

Jun JH, Ha CM, Fletcher JC (2010) BLADE-ON-PETIOLE1 coordinates organ determinacy and axial polarity in *Arabidopsis* by directly activating ASYMMETRIC LEAVES2. Plant Cell **22**: 62–76

Khan M, Xu H, Hepworth SR (2014) BLADE-ON-PETIOLE genes: setting boundaries in development and defense. Plant Sci **215–216**: 157–171

Koch B, Evans HJ (1966) Reduction of acetylene to ethylene by soybean root nodules. Plant Physiol **41**: 1748–1750

Kondorosi E, Banfalvi Z, Kondorosi A (1984) Physical and genetic analysis of a symbiotic region of Rhizobium meliloti: identification of nodulation genes. Mol Gen Genet **193**: 445–452

Kouchi H, Imaizumi-Anraku H, Hayashi M, Hakoyama T, Nakagawa T, Umehara Y, Suganuma N, Kawaguchi M (2010) How many peas in a pod? Legume genes responsible for mutualistic symbioses underground. Plant Cell Physiol **51**: 1381–1397

Krall L, Wiedemann U, Unsin G, Weiss S, Domke N, Baron C (2002) Detergent extraction identifies different VirB protein subassemblies of the type IV secretion machinery in the membranes of Agrobacterium tumefaciens. Proc Natl Acad Sci USA **99**: 11405–11410

Laporte P, Lepage A, Fournier J, Catrice O, Moreau S, Jardinaud MF, Mun JH, Larrainzar E, Cook DR, Gamas P, (2014) The CCAAT box-binding

transcription factor NF-YA1 controls rhizobial infection. J Exp Bot **65**: 481–494

Lerouge P, Roche P, Fauche C, Maillet F, Truchet G, Promé JC, Dénarié J (1990) Symbiotic host-specificity of *Rhizobium meliloti* is determined by a sulphated and acylated glucosamine oligosaccharide signal. Nature **344**: 781–784

Le Roux C, Del Prete S, Boutet-Mercey S, Perreau F, Balague C, Roby D, (2014) The hnRNP-Q protein LIF2 participates in the plant immune response. PLoS ONE **9**: e99343

Levesque MP, Vernoux T, Busch W, Cui H, Wang JY, Blilou I, Hassan H, Nakajima K, Matsumoto N, Lohmann JU, (2006) Whole-genome analysis of the SHORT-ROOT developmental pathway in Arabidopsis. PLoS Biol **4**: e143

Magne K, George J, Berbel Tornero A, Broquet B, Madueño F, Andersen SU, Ratet P (2018) *Lotus japonicus NOOT-BOP-COCH-LIKE1* is essential for nodule, nectary, leaf and flower development. Plant J **94**: 880–894

Mähönen AP, Ten Tusscher K, Siligato R, Smetana O, Díaz-Triviño S, Salojärvi J, Wachsman G, Prasad K, Heidstra R, Scheres B (2014) PLETHORA gradient formation mechanism separates auxin responses. Nature **515**: 125–129

Maillet F, Poinsot V, André O, Puech-Pagès V, Haouy A, Gueunier M, Cromer L, Giraudet D, Formey D, Niebel A, (2011) Fungal lipochitooligosaccharide symbiotic signals in arbuscular mycorrhiza. Nature **469**: 58–63

Mou Z, Fan W, Dong X (2003) Inducers of plant systemic acquired resistance regulate NPR1 function through redox changes. Cell **113**: 935–944

Norberg M, Holmlund M, Nilsson O (2005) The *BLADE ON PETIOLE* genes act redundantly to control the growth and development of lateral organs. Development **132**: 2203–2213

Oldroyd GED (2013) Speak, friend, and enter: signalling systems that promote beneficial symbiotic associations in plants. Nat Rev Microbiol **11**: 252–263

Oldroyd GED, Downie JA (2008) Coordinating nodule morphogenesis with rhizobial infection in legumes. Annu Rev Plant Biol **59**: 519–546

Olsen JL, Rouzé P, Verhelst B, Lin YC, Bayer T, Collen J, Dattolo E, De Paoli E, Dittami S, Maumus F, (2016) The genome of the seagrass Zostera marina reveals angiosperm adaptation to the sea. Nature **530**: 331–335

Osipova MA, Dolgikh EA, Lutova LA (2011) Features of the expression of a meristem-specific WOX5 gene during nodule organogenesis in legumes. [in Russian] Ontogenez **42**: 264–275

Osipova MA, Mortier V, Demchenko KN, Tsyganov VE, Tikhonovich IA, Lutova LA, Dolgikh EA, Goormachtig S (2012) *Wuschel-related homeobox5* gene expression and interaction of CLE peptides with components of the systemic control add two pieces to the puzzle of autoregulation of nodulation. Plant Physiol **158**: 1329–1341

Ovchinnikova E, Journet E, Chabaud M, Cosson V, Duc G, Fedorova E, Liu W, den Camp RO, Zhukov V, Tikhonovich I, (2011) IPD3 controls the formation of nitrogen-fixing symbiosomes in pea and Medicago spp. Mol Plant Microbe Interact **24**: 1333–1344

Pate JS (1976) Transport in symbiotic systems fixing nitrogen. *In* Transport in Plants II: Part B, Tissues and Organs. Encyclopedia of Plant Physiology, New Series, Vol 2. pp 278–303

Pate JS (1976) Transport in Symbiotic Systems Fixing Nitrogen. In: Lüttge U., Pitman M.G. (eds) Transport in Plants II. Encyclopedia of Plant Physiology (New Series), vol 2 / B. Springer, Berlin, Heidelberg 10.1007/978-3-642-66230-0_6

Pichon M, Journet E, Dedieu A, De Billy F, Truchet G, Barker DG (1992) Rhizobium meliloti elicits transient expression of the early nodulin gene ENOD12 in the differentiating root epidermis of transgenic alfalfa. Plant Cell **4**: 1199–1211

Plet J, Wasson A, Ariel F, Le Signor C, Baker D, Mathesius U, Crespi M, Frugier F (2011) MtCRE1-dependent cytokinin signaling integrates bacterial and plant cues to coordinate symbiotic nodule organogenesis in Medicago truncatula. Plant J **65**: 622–633

Putnoky P, Grosskopf E, Ha DT, Kiss GB, Kondorosi A (1988) *Rhizobium* fix genes mediate at least two communication steps in symbiotic nodule development. J Cell Biol **106**: 597–607

Putnoky P, Petrovics G, Kereszt A, Grosskopf E, Ha DTC, Bánfalvi Z, Kondorosi A (1990) *Rhizobium meliloti* lipopolysaccharide and exopolysaccharide can have the same function in the plant-bacterium interaction. J Bacteriol **172**: 5450–5458

Roux B, Rodde N, Jardinaud MF, Timmers T, Sauviac L, Cottret L, Carrère S, Sallet E, Courcelle E, Moreau S, (2014) An integrated analysis of plant and bacterial gene expression in symbiotic root nodules using laser-capture microdissection coupled to RNA sequencing. Plant J **77**: 817–837

Smith SE, Read DJ (2008) Mycorrhizal Symbiosis, Ed 3. Academic Press, New York

Soltis DE, Soltis PS, Morgan DR, Swensen SM, Mullin BC, Dowd JM, Martin PG (1995) Chloroplast gene sequence data suggest a single origin of the predisposition for symbiotic nitrogen fixation in angiosperms. Proc Natl Acad Sci USA **92**: 2647–2651

Soyano T, Kouchi H, Hirota A, Hayashi M (2013) NODULE INCEPTION directly targets NF-Y subunit genes to regulate essential processes of root nodule development in Lotus japonicus. PLoS Genet **9**: e1003352

Stahl Y, Wink RH, Ingram GC, Simon R (2009) A signaling module controlling the stem cell niche in Arabidopsis root meristems. Curr Biol **19**: 909–914

Suzaki T, Yoro E, Kawaguchi M (2015) Leguminous plants: inventors of root nodules to accommodate symbiotic bacteria. Int Rev Cell Mol Biol **316**: 111–158

Szabados L, Charrier B, Kondorosi A, de Bruijn FJ, Ratet P (1995) New plant promoter and enhancer testing vectors. Mol Breeding **1**: 419–423

Tamura K, Stecher G, Peterson D, Filipski A, Kumar S (2013) MEGA6: Molecular Evolutionary Genetics Analysis version 6.0. Mol Biol Evol **30**: 2725–2729

Tang H, Krishnakumar V, Bidwell S, Rosen B, Chan A, Zhou S, Gentzbittel L, Childs KL, Yandell M, Gundlach H, (2014) An improved genome release (version Mt4.0) for the model legume *Medicago truncatula*. BMC Genomics **15**: 312

Truchet G, Camut S, de Billy F, Odorico R, Vasse J (1989) The Rhizobium-legumes symbiosis: two methods to discriminate between nodules and other root-derived structures. Protoplasma **149**: 82–88

Udvardi M, Poole PS (2013) Transport and metabolism in legume-rhizobia symbioses. Annu Rev Plant Biol **64**: 781–805

Van de Velde W, Guerra JC, De Keyser A, De Rycke R, Rombauts S, Maunoury N, Mergaert P, Kondorosi E, Holsters M, Goormachtig S (2006) Aging in legume symbiosis: a molecular view on nodule senescence in *Medicago truncatula*. Plant Physiol **141**: 711–720

Vasse J, de Billy F, Camut S, Truchet G (1990) Correlation between ultrastructural differentiation of bacteroids and nitrogen fixation in alfalfa nodules. J Bacteriol **172**: 4295–4306

Wang Q, Hasson A, Rossmann S, Theres K (2016) Divide et impera: boundaries shape the plant body and initiate new meristems. New Phytol **209**: 485–498

Weber E, Engler C, Gruetzner R, Werner S, Marillonnet S (2011) A modular cloning system for standardized assembly of multigene constructs. PLoS ONE **6**: e16765

Wellensiek SJ (1959) Neutronic mutations in peas. Euphytica **8**: 209–215

Werner GDA, Cornwell WK, Sprent JI, Kattge J, Kiers ET (2014) A single evolutionary innovation drives the deep evolution of symbiotic N2-fixation in angiosperms. Nat Commun **5**: 4087

Xiao TT, Schilderink S, Moling S, Deinum EE, Kondorosi E, Franssen H, Kulikova O, Niebel A, Bisseling T (2014) Fate map of *Medicago truncatula* root nodules. Development **141**: 3517–3528

Yaxley JL, Jablonski W, Reid JB (2001) Leaf and flower development in pea (Pisum sativum L.): mutants cochleata and unifoliate. Ann Bot (Lond) **88**: 225–234

Žádníková P, Simon R (2014) How boundaries control plant development. Curr Opin Plant Biol **17**: 116–125